Atmos. Chem. Phys. Discuss., https://doi.org/10.5194/acp-2017-826
Manuscript under review for journal Atmos. Chem. Phys.
Discussion started: 13 October 2017

Atmospheric Chemistry and Physics Discussions

A European aerosol phenomenology-6: Scattering properties of atmospheric aerosol particles from 28 ACTRIS sites

Marco Pandolfi[1], Lucas Alados-Arboledas[2], Andrés Alastuey[1], Marcos Andrade[3], Begoña Artiñano[4], John Backman[5,6], Urs Baltensperger[7], Paolo Bonasoni[8], Nicolas Bukowiecki[7], Martine Collaud Coen[9], Sebastian Conil[10], Esther Coz[4], Vincent Crenn[11,12], Vadimas Dudoitis[13], Marina Ealo[1], Kostas Eleftheriadis[14], Olivier Favez[15], Prodromos Fetfatzis[14], Markus Fiebig[16], Harald Flentje[17], Patrick Ginot[18], Martin Gysel[7], Bas Henzing[19], Andras Hoffer[20], Adela Holubova Smejkalova[21,22], Ivo Kalapov[23], Nokos Kalivitis[24,25], Giorgos Kouvarakis[24], Adam Kristensson[26], Markku Kulmala[5], Heikki Lihavainen[6], Chris Lunder[16], Krista Luoma[5], Hassan Lyamani[2], Angela Marinoni[8], Nikos Mihalopoulos[24,25], Marcel Moerman[19], José Nicolas[27], Colin O'Dowd[28], Tuukka Petäjä[5], Jean-Eudes Petit[11,15], Jean Marc Pichon[27], Nina Prokopciuk[13], Jean-Philippe Putaud[29], Sergio Rodríguez[30], Jean Sciare[11,a], Karine Sellegri[27], Dimiter B. Stamenov[23], Erik Swietlicki[26], Gloria Titos[1,2], Thomas Tuch[31], Peter Tunved[32], Vidmantas Ulevicius[13], Aditya Vaishya[28,33], Milan Vana[21,22], Aki Virkkula[5], Stergios Vratolis[14], Ernest Weingartner[7,b], Alfred Wiedensohler[31], and Paolo Laj[5,8,18]

[1] *Institute of Environmental Assessment and Water Research, c/ Jordi-Girona 18-26, 08034, Barcelona, Spain*
[2] *Andalusian Institute for Earth System Research, IISTA-CEAMA, University of Granada, Granada 18006, Spain*
[3] *Atmospheric Physics Laboratory, ALP, UMSA, Campus Cota Cota calle 27, Endifico FCPN piso 3, La Paz, Bolivia*
[4] *Centro de Investigaciones Energéticas, Medioambientales y Tecnológicas, CIEMAT, Unidad Asociada en Contaminación Atmosférica, CIEMAT-CSIC, Avda. Complutense, 40, 28040 Madrid*
[5] *University of Helsinki, UHEL, Division of Atmospheric Sciences, PO BOX 64, FI-00014, Helsinki, Finland*
[6] *Finnish Meteorological Institute, FMI, Erik Palmenin aukio 1, FI-00560, Helsinki, Finland*
[7] *Paul Scherrer Institut, PSI, Laboratory of Atmospheric Chemistry (LAC), OFLB, , 5232, Villigen PSI, Switzerland*
[8] *Institute of Atmospheric Sciences and Climate, ISAC, Via P. Gobetti 101, I-40129, Bologna, Italy*
[9] *Federal Office of Meteorology and Climatology, MeteoSwiss, Chemin de l'aérologie, 1530 Payerne, Switzerland*
[10] *ANDRA – DRD – Observation Surveillance, Observatoire Pérenne de l'Environnement, Bure, France*
[11] *LSCE-Orme point courrier 129 CEA-Orme des Merisiers, 91191 Gif-sur-Yvette, France*
[12] *ADDAIR, BP 70207 - 189, rue Audemars, 78530, Buc, France*
[13] *SRI Center for Physical Sciences and Technology, CPST, Sauletekio ave. 3, LT-10257, Vilnius, Lithuania*
[14] *Institute of Nuclear & Radiological Science & Technology, Energy & Safety, N.C.S.R. "Demokritos", Athens, 15341, Greece*
[15] *Institut National de l'Environnement Industriel et des Risques, Verneuil en Halatte, 60550, France*
[16] *Norwegian Institute for Air Research, Atmosphere and Climate Department, NILU, Instituttveien 18, , 2007, Kjeller, Norway*
[17] *Deutscher Wetterdienst, Met. Obs. Hohenpeissenberg, DE-82383 Hohenpeissenberg, Germany*
[18] *Univ. Grenoble-Alpes, CNRS, IRD, INPG, IGE F-38000 Grenoble, France*
[19] *TNO B&O, Princetonlaan 6, 3584TA, The Hague, The Netherlands*
[20] *MTA-PE Air Chemistry Research Group, Veszprém, P.O. Box 158, H-8201, Hungary*
[21] *Global Change Research Institute AS CR, Belidla 4a, 603 00, Brno, Czech Republic*
[22] *Czech Hydrometeorological Institute, Na Sabatce 17 , 143 06, Praha, Czech Republic.*
[23] *Institute for Nuclear Research and Nuclear Energy, Basic Environmental Observatory Moussala, 72 Tsarigradsko Chaussee Blvd, 1784-Sofia, Bulgaria*
[24] *Environmental Chemical Processes Laboratory, Dept. of Chemistry, Univ. of Crete, Heraklion, 71003, Greece*
[25] *Institute for Environmental Research & Sustainable Development, National Observatory of Athens (NOA), I. Metaxa & Vas. Pavlou, 15236 Palea Penteli, Greece*

[26] *Lund University, Department of Physics, P. O. Box 118, SE-22100, Lund, Sweden*
[27] *CNRS-LaMP Université Blaise Pascal 4, Avenue Blaise Pascal 63178 Aubiere Cedex, France*
[28] *School of Physics and Centre for Climate & Air Pollution Studies, Ryan Institute, National University of Ireland Galway, University Road, Galway, Ireland*
[29] *EC Joint Research Centre, EC-JRC-IES, Institute for Environment and Sustainability, Via Enrico Fermi 2749, 21027, Ispra, Italy*
[30] *Agencia Estatal de Meteorologia, AEMET, Izaña Atmospheric Research Center, La Marina 20, E-38071, Santa Cruz de Tenerife, Spain*
[31] *Leibniz Institute for Tropospheric Research, (TROPOS), Permoserstraße 15, 04318, Leipzig, Germany*
[32] *Department of Environmental Science and Analytical Chemistry (ACES) and the Bolin Centre for Climate Research, Stockholm University, SE-106 91 Stockholm, Sweden*
[33] *Space Physics Laboratory, Vikram Sarabhai Space Centre, ISRO, Thiruvananthapuram – 695022, India.*

[a] *now at: EEWRC, The Cyprus Institute, Nicosia, Cyprus*
[b] *now at: Institute for Aerosol and Sensor Technology, University of Applied Sciences (FHNW), Windisch, Switzerland*

Atmos. Chem. Phys. Discuss., https://doi.org/10.5194/acp-2017-826
Manuscript under review for journal Atmos. Chem. Phys.
Discussion started: 13 October 2017

Atmospheric Chemistry and Physics Discussions

Abstract

This paper presents the light scattering properties of atmospheric aerosol particles measured over the past decade at 28 ACTRIS observatories, located mainly in Europe. The data include particle light scattering (σ_{sp}) and hemispheric backscattering (σ_{bsp}) coefficients, scattering Ångström exponent (SAE), backscatter fraction (BF) and asymmetry parameter (*g*). A large range of σ_{sp} was observed across the network. Low σ_{sp} values were on average measured in Nordic and Baltic countries and in Western Europe whereas the highest σ_{sp} were measured at regional sites in eastern and central Europe. In these regional areas the SAE was also high indicating the predominance of fine-mode particles. On average, the SAE was lower in the Nordic and Baltic, western and southern countries suggesting a lower fraction of fine-mode particle compared to central and eastern Europe. An increasing gradient of σ_{sp} was observed when moving from mountain to regional and to urban sites. Conversely, the mass-independent SAE and *g* parameters did not show the same gradient. At all sites, both SAE and *g* varied greatly with aerosol particle loading. The lowest values of *g* were always observed under low σ_{sp} indicating a larger contribution from particles in the smaller accumulation mode. Then, *g* steeply increased with increasing σ_{sp} indicating a progressive shift of the particle size distribution toward the larger end of the accumulation mode. Under periods of high particle mass concentrations, the variation of *g* was less pronounced whereas the SAE increased or decreased suggesting changes mostly in the coarse aerosol particles mode rather than in the fine mode. The station placement seemed to be the main parameter affecting the intra-annual variability. At mountain sites, higher σ_{sp} was measured in summer mainly because of the enhanced boundary layer influence. Conversely, less horizontal and vertical dispersion in winter led to higher σ_{sp} at all low altitude sites in central and eastern Europe compared to summer. On average, these sites also showed SAE maxima in summer (and correspondingly *g* minima). Large intra-annual variability of SAE and *g* was observed also at Nordic and Baltic countries due to seasonal-dependent transport of different air masses to these remote sites. Statistically significant decreasing trends of σ_{sp} were observed at 5 out of 13 stations included in trend analyses. The total reductions of σ_{sp} were consistent with those reported for $PM_{2.5}$ and PM_{10} mass concentrations over similar periods across Europe.

Atmos. Chem. Phys. Discuss., https://doi.org/10.5194/acp-2017-826
Manuscript under review for journal Atmos. Chem. Phys.
Discussion started: 13 October 2017

Atmospheric Chemistry and Physics Discussions

1. Introduction

Atmospheric aerosol particles are recognized as an important atmospheric constituent with demonstrated effects on climate and health. Radiative forcing of aerosol particles, estimated as –0.9 [–1.9 to −0.1] W/m^2 (IPCC, 2014), has two competing components: a cooling effect from most particle types and a partially offsetting warming contribution from black carbon (BC) particle light absorption of solar radiation. The aerosol cooling is the dominant effect; thus aerosol particles are counteracting a substantial portion of warming effect from well mixed greenhouse gases (GHGs). This process is driven by the scattering properties of most aerosol particle types (e.g. secondary sulfate and nitrate particles, mineral and organic matter), which reduces the amount of solar radiation reaching the Earth surface reflecting it back to space and modifying the Earth's radiative balance. However, the high temporal and spatial variability of atmospheric aerosol particles, due to the wide variety of aerosol sources and sinks, their short and variable lifetime (hours to weeks in the planetary boundary layer) and spatial non-uniformity, contribute to the largest uncertainty in the estimation of the total radiative forcing. Reducing these uncertainties is mandatory in view of global warming experienced over the past 50 years. In fact, there are evidences suggesting that the observed (and projected) decrease in emissions of anthropogenic aerosol particles, in response to air quality policies, would eventually unmask the global warming (Rotstayn et al., 2013). Thus, current emission controls could increase climate warming while improving air quality (e.g. Stohl et al., 2015). The measurements of aerosol particle optical properties such as light scattering and absorption, together with measurements of physical and chemical properties, are fundamental in order to better understand the current conflict involving a trade-off between the impacts of aerosols on environmental health and Earth's climate. Several international projects are providing in the last decades important information on the atmospheric particle properties worldwide. Near-surface in-situ observations of aerosol particle properties are performed worldwide under the GAW/WMO program completed with policy-oriented programs such as IMPROVE (Interagency Monitoring of Protected Visual Environments; http://vista.cira.colostate.edu/Improve/) in USA or EMEP (European Monitoring and Evaluation Programme; http://www.emep.int/) in Europe. Additional information specifically targeting advanced aerosol particle properties are obtained in Europe using information from the European research infrastructure ACTRIS (Aerosols, Clouds, and Trace gases Research InfraStructure; http://www.actris.eu) or from short-term RTD projects such as EUCAARI (European Integrated Project on Aerosol Cloud Climate and Air Quality Interactions; http://www.cas.manchester.ac.uk/resprojects/eucaari/). The implementation of the GAW program in Europe is performed under ACTRIS for the advanced observation of aerosol particle properties. ACTRIS is providing harmonized measurement of different (physical, chemical and optical) aerosol properties in a systematic way at major observation sites in Europe. More than 60 measuring sites worldwide are currently providing ground-based in-situ aerosol particle light scattering measurements (EBAS database; www. http://ebas.nilu.no/) and the number has increased substantially in the last decade.

The objective of this work is to integrate the total aerosol light scattering coefficient (σ_{sp}) and hemispheric backscattering coefficient (σ_{bsp}) measurements performed over several years at the ground based in-situ ACTRIS stations. A total of 28 stations (25 European + 3 non-European) are included in order to document the variability in near-surface aerosol particle light scattering across the ACTRIS network. Moreover, at some of the ACTRIS stations more than 10 years of σ_{sp} data are available allowing us to perform trends analysis. The study of the trend of σ_{sp} is important given that decreasing or increasing trend of σ_{sp} would mirror the effectiveness of the air quality control measures. In fact, many studies have shown that the concentrations of particulate matter (PM), and other air pollutants such as sulfur dioxide (SO_2) and carbon monoxide (CO), have clearly decreased during the last 20 years in many European Countries (Barmpadimos et al., 2012; Cusack et al., 2012; EEA, 2013; Querol et al., 2014; Guerreiro et al., 2014; Pandolfi et al., 2016, Tørseth et al., 2012, among others).

Previous studies presenting multi-site ground-based in-situ aerosol particle optical measurements were for example performed by Delene and Ogren (2002), Collaud Coen et al. (2013) and Andrews et al. (2011). Delene and Ogren (2002) reported the variability of aerosol particle optical properties at four North American surface monitoring sites. Collaud Coen et al. (2013) presented long term (>8-9 years) aerosol particle light scattering and absorption measurements performed at 24 regional/remote observatories, among which 5 of them are located in Europe. Andrews et al. (2011) reported the aerosol particle optical measurements performed at 12 (4 located in Europe) mountain top observatories. Thus, the number of papers reporting aerosol particle optical properties measured at different sites is rather scarce and unfortunately almost inexistent outside Europe and the United States.

Our work is focused mainly on European observatories aiming at a representative phenomenology of aerosol particle light scattering coefficient measured at ACTRIS stations. Thanks to the establishment of European monitoring networks and/or research projects five papers have been published related with aerosol phenomenology in Europe: Van Dingenen et al. (2004) and Putaud et al. (2004) on the physical and chemical, respectively, characteristics of particulate matter (PM) at kerbside, urban, rural and background sites in Europe; Putaud et al. (2010) on the physical and chemical characteristics of PM measured at 60 sites across Europe; Cavalli et al. (2016) on the harmonized concentrations of carbonaceous aerosol at ten regional background sites in Europe; Zanatta et al. (2016) presenting a climatology of BC optical properties at nine European regional background sites. The importance of these studies and of the present work relies on the evidence that a reliable assessment of the physical, chemical and optical properties of aerosol particles at European scale is of crucial importance for an accurate estimation of the radiative forcing of atmospheric aerosols. This work is the first European phenomenology study dedicated to the light scattering properties of aerosol particles measured in-situ at near-surface ground-based observatories. Moreover, the trend analyses presented can be used to evaluate how the European mitigation strategies adopted to improve air quality affected the aerosol particle optical properties.

In fact, starting from the σ_{sp} measurements performed at the ACTRIS observatories, three intensive aerosol particle optical parameters can be estimated, namely the scattering Ångström exponent (SAE), the backscattering fraction (BF), and the asymmetry parameter (*g*). These intensive properties do not depend on the PM mass concentration and are directly related to aerosol particles properties such as size, shape, size distribution and chemical composition. The SAE can be considered a proxy for the aerosol particle size range with higher (lower) SAE associated to predominance of fine (course) aerosol particles (e.g. Seinfeld and Pandis, 1998; Esteve et al., 2012; A. Valenzuela et al., 2015 among others). The BF and *g* parameters are calculated quantities that influence the variability of the radiative forcing efficiency and that represent the angular light scattering of aerosol particles. For computational efficiency, the angular light scattering is often represented by a single value (BF, σ_{sp}/σ_{bsp} or *g*) (Ogren et al., 2006). For some of the ACTRIS data used in this work, trends of these intensive aerosol particle optical properties are investigated as well.

2. Experimental

2.1 Atmospheric Observatories

Figure 1 shows the location of the observatories which are grouped based on their geographical location as performed in other European phenomenology studies (e.g. Putaud et al., 2010). Observatories information and measurements periods are summarized in Table 1. The observatories are also divided in five different categories depending on their placement in each geographical sector. Mountain: includes those observatories located at more than 1 km above sea level; coastal: includes observatories located close to the sea coast; regional: includes those observatories mostly affected by regional sources and closer to large pollution sources compared to continental sites; continental: comprise observatories located in remote continental areas; urban/sub-urban: includes observatories located in urban background or suburban areas.

Nordic and Baltic stations are represented by Birkenes (BIR, Norway; regional), Hyytiälä (SMR, Finland; regional), Pallas (PAL, Finland; continental), Vavihill (VHL, Sweden; continental), and Preila (PLA, Lithuania; coastal). Western European sites are Puy De Dome (PUY, France; mountain), Mace Head (MHD, Ireland; coastal), Cabauw (CBW, The Netherlands; regional), SIRTA (SIR, France; suburban), and Observatory Perenne (OPE, France; regional). Central European stations are Jungfraujoch (JFJ, Switzerland; mountain), Hohenpeissenberg (HPB, Germany; mountain), Melpitz (MPZ, Germany; regional), Ispra (IPR, Italy; semi regional), Mt. Cimone (CMN, Italy; mountain) and Košetice (KOS, Czech Republic; regional). Eastern European stations are Beo Moussala (BEO, Bulgaria; mountain) and K-Puszta (KPS, Hungary; regional). South-western European stations are represented by Izaña (IZO, Spain; mountain), Montsec (MSA, Spain; mountain), Montseny (MSY, Spain; regional), Madrid (MAD, Spain; sub-urban), and Granada

(UGR, Spain; urban) whereas south-eastern European stations are Athens (DEM, Greece; sub-urban) and Finokalia (FKL, Greece; coastal). Finally, Arctic and Antarctic stations are Zeppelin (ZEP) and Troll (TRL), respectively. Another non-European mountain station included is Mt. Chacaltaya (CHC, Bolivia; mountain). The altitude of the mountain stations considered here ranges between 985 m at HPB to 5240 m at CHC. Some of the mountain stations included in this investigation have been already included in the work by Andrews et al. (2011), namely IZO, JFJ, CMN, and BEO. Moreover, FKL, HPB, JFJ, MHD, and PAL stations have been included in the study by Collaud Coen et al. (2013). Both studies presented in-situ aerosol particle optical measurements performed at these stations. Main results from the previous investigation are summarized in the results section.

At JFJ, HPB, IPR (Central Europe), UGR (southwestern Europe), MHD (western Europe), PAL and SMR (Nordic and Baltic), at least 10 years of data are available for trend analysis. However, in order to improve the spatial coverage, trends are also studied at CMN, MPZ (central Europe), IZO (southwestern Europe), PUY (western Europe), KPS and BEO (eastern Europe), where >8-9 years of data are available (cf. Table 1). The stations included in this work report the data to ACTRIS and GAW/EMEP, consequently the data are quality assured given that the nephelometer instruments are run following the ACTRIS/GAW standards (WMO-GAW Report, 2016) and regularly inter-compared.

2.2 Scattering measurements

2.2.1 Instruments

The measurements of σ_{sp} and σ_{bsp} included in this study were obtained from TSI and Ecotech integrating nephelometers (Table 1). These optical instruments measure the amount of light scattered by particles in the visible spectrum and provide σ_{sp} and σ_{bsp} coefficients of sampled aerosols. Most used nephelometer models are the TSI3563 and the Ecotech AURORA3000, both providing σ_{sp} and σ_{bsp}. Model TSI3563 measures σ_{sp} and σ_{bsp} at 450, 550, and 700 nm whereas the Ecotech AURORA3000 measures at 450, 525 and 635 nm. Other used models are the M9003 from Ecotech (SIR and CMN) and the RR (Radiance Research) nephelometer model M903 (FKL) measuring σ_{sp} at 520 nm and 532 nm, respectively. Due to the non-homogeneity of the light source of the model M9003, the light source was changed at SIR in 2013 with the AURORA3000 light source and at CMN in 2009 with an opal glass light source. The detailed description of the main characteristics and working principle of the integrating nephelometers can be found e.g. in Müller et al. (2011) for the Ecotech AURORA3000 and in Anderson and Ogren (1998) for the model TSI 3563. Following the ACTRIS and WMO-GAW recommendations, the nephelometers are regularly calibrated using span gas and zero-adjusted using particle-free air. Recommended quality assurance procedures during on-site operation as described in GAW (WMO/GAW, 2016), guarantee the quality and comparability of the data. Moreover, most of the integrating

nephelometers involved in ACTRIS have undergone performance checks at scheduled times at the World Calibration Center for Aerosol Physical properties of ACTRIS/GAW.

2.2.2 Data treatment

2.2.2.1 Truncation correction

Data from integrating nephelometers used here are corrected for non-ideal illumination of the light source (deviation from Lambertian distribution of light) and for truncation of the sensing volumes in the near-forward (around 0-10º) and near-backward direction (around 170-180º) (Müller et al., 2009 and Anderson and Ogren, 1998). Correction schemes have been provided by Müller et al. (2011) for the Ecotech AURORA3000 and by Anderson and Ogren (1998) for the TSI3563. Both methods provide a simple linear correction scheme based on the scattering Ångström exponent (SAE) determined from raw nephelometer data to correct for the size distribution-dependent truncation error. It has been demonstrated that for an aerosol particle population with a single scattering albedos (SSA) greater than 0.8 this simple correction scheme provides a suitable quantification of the truncation error (Müller et al., 2011). However, for SSA < 0.8 a correction scheme based on particle number size distribution should be used (Müller et al., 2011). The aerosol particle light scattering data used here are corrected for non-ideal illumination and for truncation by the data providers or in this work. This information is reported in Table S1 of the Supporting Material. Only at SIR, FKL, and CMN, σ_{sp} data are not corrected for truncation because σ_{sp} at these observatories was measured at one wavelength. At CMN, the 3-λ TSI3563 is operative since 2014 (cf. Table 1). However, not correcting for truncation doesn't prevent from comparing non-corrected σ_{sp} with truncation corrected σ_{sp}. The truncation correction increases with particle size being more important for coarse aerosol particles. For example, using the SAE calculated at CMN for the years 2014-2015 and the correction scheme provided for the TSI3563 by Anderson and Ogren (1998), the difference between non-corrected σ_{sp} and corrected mean σ_{sp} is lower than 7% at this site.

2.2.2.2 Relative humidity

The integrating nephelometer measurements within ACTRIS and WMO-GAW should be performed at low relative humidity (RH) in order to avoid enhanced scattering due to water uptake of aerosol particles and to make measurements comparable. For the Ecotech integrating nephelometers the RH threshold can be set by using a processor-controlled automatic heater inside the nephelometer. At some mountain sites where whole air is sampled (cf. Table 1), the natural temperature difference between outside and inside air dries cloud droplets to the aerosol phase when a cloud is present at the station. RH is also controlled by de-humidifying in the inlet pipe as

reported in the GAW report 226 to ensure sampling RH of less than 40%. This recommendation intends to make the data comparable across the network, which otherwise would be a strong function of the highly variable sample RH. Currently, at the majority of ACTRIS observatories, the aerosol particles light scattering measurements are performed at RH lower than 40%. However, given that at some stations the 40% RH threshold is sometimes exceeded, we selected in this work a RH threshold of 50% in order to improve the data coverage. Estimating the aerosol particle light scattering enhancement due to an increase of RH from 40% to 50% is difficult using the data available here because σ_{sp} measurements at RH>40% are not evenly distributed over the measurement periods. In fact, at the majority of the stations RH higher than 40% is registered mostly in summer. However, the scattering enhancement due to a change in RH between 40% and 50% should be small and will not exceed around 3-5% even for more hygroscopic particles (e.g. Fierz-Schmidhauser et al., 2010a,b). Table S2 in the Supporting Material reports the number of RH hourly data reported at each observatory and the number and % of hourly RH data >50%. The frequency distributions of measured RH are shown in Figure S1. Finally, σ_{sp} and σ_{bsp} data reported to EBAS and used in this work are referenced to standard T (273.15 ºC) and P (1013 hPa) conditions.

2.2.2.3 Available wavelengths

In this work we present and discuss the σ_{sp}, BF and *g* measurements obtained using the green wavelength of the integrating nephelometers. The available wavelengths ranged from 520 nm (2 stations, CMN and VHL) to 550 nm (18 stations). Other used wavelengths are 525 nm (6 stations), 532 nm (used at FKL until 2010; cf. Table 2). An exception is SIR where only σ_{sp} at 450 nm is available. The measurements of σ_{sp} reported here are not adjusted to 550 nm which generally is the most used wavelength (e.g. Andrews et al., 2011) because of the different data availability of σ_{sp} and SAE at the measuring stations. As discussed in the following Sections SAE is calculated for σ_{sp} data higher than 0.8 Mm^{-1}, thus leading to different data coverage for σ_{sp} and SAE and thus preventing the adjustment of all measured σ_{sp} to 550 nm. Moreover, SAE is not available at FKL and SIR (and at CMN until 2014) thus preventing any wavelength adjustment at these stations. Using the mean SAE calculated at those stations where σ_{sp} is measured at different wavelength than 550 nm (cf. Tables S4 and S5 in Supporting material), we estimate differences in σ_{sp} lower than 6% after adjusting to 550 nm. At FKL and SIR, where SAE is not available and assuming a SAE of 1.5, the difference by adjusting to 550 nm is 4.9% at FKL and 26% at SIR, respectively. The higher difference at SIR is due to the fact that measurements at this station are performed at 450 nm. Finally, at CMN the effect of the adjustment of σ_{sp} to 550 nm (from 520 nm) using a mean SAE of 2 (cf. Table S5) is lower than 10%.

Atmos. Chem. Phys. Discuss., https://doi.org/10.5194/acp-2017-826
Manuscript under review for journal Atmos. Chem. Phys.
Discussion started: 13 October 2017

Atmospheric Chemistry and Physics Discussions

2.2.3 Calculation of aerosol particle intensive optical properties

In addition to the direct σ_{sp} and σ_{bsp} measurements obtained with the above detailed instrumentation, the following aerosol intensive parameters are calculated from hourly-averaged in-situ data.

The scattering Ångström exponent (SAE) characterizes the wavelength dependency of σ_{sp} and it can be calculated as follows (with $\lambda_1 > \lambda_2$):

$$SAE = -\frac{\log\left(\sigma_{sp}^{\lambda_1} / \sigma_{sp}^{\lambda_2}\right)}{\log\left(\lambda_1 / \lambda_2\right)} \quad \text{(Eq. 1)}$$

Here, the SAE is calculated as linear estimation of σ_{sp} measured at the three available wavelengths. The SAE depends on particle size distribution. It takes values greater than 2 when the light scattering is dominated by fine particles (radii ≤ 0.5 μm as e.g. in Schuster et al. (2006)), while it is lower than one when the light scattering is increasingly dominated by coarse particles (Seinfeld and Pandis, 1998; Schuster et al., 2006).

The asymmetry parameter (*g*) (Andrews et al., 2006; Delene and Ogren, 2002) describes the probability that the radiation is scattered in a given radiation and it is defined as the cosine-weighted average of the phase function. Thus, *g* gives information on the amount of radiation that a particle can scatter in the forward direction compared to the backward direction. Theoretically, the values of *g* can range from −1 for only back scattering to +1 for complete forward scattering (0º), with a value of 0.7 commonly used in radiative transfer models (Ogren et al., 2006). The g parameter can be estimated from the backscatter fraction (BF) which is the ratio between σ_{bsp} and σ_{sp} (Andrews et al., 2006):

$$g = -7.14(BF)^3 + 7.46(BF)^2 - 3.96(BF) + 0.9893 \quad \text{(Eq. 2)}$$

2.2.4 Data coverage

Table S3 in the Supporting Material reports the number of hours and data availability for each atmospheric observatory. The data coverage reported in Table S3, refers to scattering and backscattering measurements performed at RH<50%. The data coverage for the extensive measured aerosol particle optical properties (σ_{sp} and σ_{bsp}) is generally high ranging from around 60% to 95%. Exception are σ_{sp} measurements in the blue (450 nm) and in the red (700 nm) and σ_{bsp} measurements at CMN where the three wavelengths nephelometer was implemented starting from 2014. Consequently, also SAE and *g* has low data coverage at CMN. Moreover, lower data coverage (< 40%) was registered at PLA and VHL. The data coverage for the intensive aerosol particle optical properties (SAE and *g*) is generally lower compared to the data coverage of σ_{sp} and

σ_{bsp}. This is because the intensive optical properties are calculated from hourly σ_{sp} and σ_{bsp} data higher than 0.8 Mm^{-1} to avoid noise in the calculations. As a consequence, the data coverage of the intensive properties is lower at those stations measuring usually low σ_{sp} and σ_{bsp} (e.g. mountain and remote sites). For example, at JFJ the SAE and *g* data coverage is of around 54% and 22%, respectively. At TRL these values are even lower, with 21% and 1%, respectively. However, as reported in Table S3, at the majority of the stations the data coverage of SAE and *g* is higher than 60%.

3. Results/Discussion

3.1 Variability of σ_{sp}

Figure 2 shows the box-and-whiskers plots of σ_{sp} measured at the stations included in this investigation. Table S4 and Figure S2 in the Supplementary Material report, respectively, the statistics of σ_{sp} (mean, standard deviation, minimum and maximum values and 5^{th}, 25^{th}, 50^{th}, 75^{th}, and 95^{th} percentiles) and frequency and cumulative frequency distributions.

In Fig. 2, data are grouped based on their geographical location (cf. Fig. 1) and ordered based on their placement, from mountain sites to urban sites. In each geographical sector, an increasing gradient of σ_{sp} is generally observed when moving from mountain to regional and to urban sites. Thus, σ_{sp} measured at mountain sites is always lower compared to measurements performed at other placements (coastal to urban) even if exceptions are observed in some sectors. A large range of σ_{sp} coefficients is observed across the network ranging from median values lower than 10 Mm^{-1} to values higher than 40 Mm^{-1}. The observed variation is consistent with the differences in particulate matter (PM) mass concentrations, PM chemical composition and particle number concentration observed across Europe as described for example by Putaud et al. (2010) and Asmi et al. (2011). Figure 3 shows the relationship between the mean particle number concentration measured at different stations during 2008 – 2009 reported in Asmi et al. (2011) and the mean σ_{sp} measured over the same period (where available). As reported in Fig. 3, a good correlation is observed between N50 (mean/median particle number between 50 nm and 500 nm) and N100 (mean/median particle number between 100 nm and 500 nm) and mean σ_{sp}. Overall, the lowest σ_{sp} is on average measured at remote stations either because of: a) their altitude, for example JFJ located in central Europe at more than 3500 m a.s.l. and CHC in Bolivia at around 5300 m a.s.l., or b) because their large distance from pollution sources, for example the coastal ZEP and TRL stations and some regional/continental sites in the Nordic and Baltic sector such as BIR, SMR and PAL. The Arctic (ZEP) and Antarctic (TRL) monitoring stations are located in undisturbed environments with minimal influence from the local settlement since these are located above the inversion layers. The PAL station (Nordic and Baltic) is located in a remote continental area and the low σ_{sp} measured at this site are mainly due to the absence of large local and regional pollution

sources (e.g. Aaltonen et al., 2006). Conversely, higher σ_{sp} (medians > 40 Mm^{-1}) are on average registered at more polluted sites such as some urban sites in southern Europe (UGR and DEM), some regional sites in eastern and central Europe (KPS and IPR, respectively), and one coastal site in the Nordic and Baltic sector (PLA). Finally, at all stations included in this work, the skewness of σ_{sp} distributions (cf. Table S4) is higher than one and ranged between 1.4 at PLA and 10.6 at TRL (skewness calculated from hourly averaged data). Positive skewness is usually observed for positive defined parameters having a frequency distribution with a pronounced right tail indicating the presence of high positive values. Figure S2 in the Supporting Material shows the frequency and cumulative frequency distributions for σ_{sp} for each station evidencing the presence of these right tails.

3.1.1 σ_{sp} at mountain observatories

Differences can be observed among stations with similar placements but different geographical locations. Among the mountain stations higher mean σ_{sp} is on average measured at HPB and IZO (cf. Table S4). HPB station is likely to be more influenced by the PBL than other mountain stations due to its lower altitude (Nyeki et al., 2012; Collaud Coen et al., 2017), whereas IZO is largely influenced by Saharan dust outbreaks transporting dust toward the station (e.g. Rodriguez et al., 2011) thus increasing σ_{sp}. In fact, at IZO the median value of σ_{sp} is among the lowest measured at these mountain sites (around 7 Mm^{-1}; cf. Table S4) indicating that sporadic but extremely intense pollution episodes due to Saharan mineral dust outbreaks strongly affect the mean σ_{sp} at this station. The lowest median σ_{sp} at mountain sites are on average measured at JFJ probably due to the higher altitude of this station compared to other mountain stations included in this work and/or the distance from important pollution sources. Moreover, Collaud Coen et al. (2017) reported a low PBL influence at this site due to the location of the station in a dominant position in the whole mountainous massif. CHC registers higher median σ_{sp} compared to IZO or JFJ despite its location at around 5300 m a.s.l. likely due to the influence of the emissions from the city of La Paz (3600 m a.s.l.) located around 30 km far from CHC and the local topography which facilitates the uplift of air masses toward the CHC observatory (Collaud Coen et al., 2017).

3.1.2 σ_{sp} at regional/continental observatories

Regional sites present a large variability in σ_{sp} coefficients across Europe with the lowest values measured at BIR and SMR (Nordic and Baltic) and the highest at IPR (central Europe) and KPS (eastern Europe). At both IPR and KPS, the frequent wintertime episodes linked to strong stable air with thermal inversion strongly affect the level of pollution at these sites (e.g. Putaud et al., 2014; Molnár et al., 2016). On the other side, it is known that the IPR station, even though it lies several tens of kilometers away from large pollution sources, is located in an area (the Po Valley) which is

one of the most polluted regions in Europe (e.g. van Donkelaar et al., 2010). Among the continental sites, VHL registers on average higher σ_{sp} compared to PAL and compared to BIR and SMR regional sites likely because VHL is located closer to the continent and it is consequently more affected by polluted continental air masses. Moreover, the emissions from densely populated areas of Helsingborg and Malmö and the city of Copenhagen located 25 km to the west, 50 km to the south, and 45 km to the south-east, respectively, could also explain the relatively high σ_{sp} measured at VHL (Kecorius et al., 2016). The σ_{sp} values at regional level in Western Europe (OPE and CBW) are on average higher compared to those measured in the Nordic and Baltic regions and lower compared to those measured at regional level in south Europe (MSY).

3.1.3 σ_{sp} at urban observatories

Among the urban background sites, lower σ_{sp} are measured at MAD and SIR compared to DEM and UGR. Low σ_{sp} at MAD during the period presented here (only 2014 available for MAD) could be related to the reduced formation of secondary nitrate aerosols due to the limitation in the availability of ammonia in this urban environment (Revuelta et al., 2014). However, it should be considered that winter episodes with high secondary nitrate concentrations are not uncommon in Madrid and we are presenting here only one year of measurements for this station. On the other hand, secondary inorganic aerosol concentrations recorded at SIR sub-urban observatory can be considered as representative of a large geographical zone, given the rather flat orography of the Parisian basin. At UGR, the accumulation, mainly in winter, of fine particles from traffic, domestic heating and biomass burning explains the relatively higher σ_{sp} (e.g. Lyamani et al., 2012; Titos et al., 2017). Traffic emissions, high formation of secondary sulfate and organic aerosols in summer together with the transport of dust from Africa are the main reasons explaining the high σ_{sp} at DEM where high $PM_{2.5}$ and PM_{10} are usually measured compared to other important Mediterranean cities (e.g.: Diapouli et al., 2017; Eleftheriadis et al., 2014; Karanasiou et al. 2014; Querol et al., 2009).

3.1.4 σ_{sp} at coastal observatories

The PLA coastal station registered σ_{sp} values higher compared to both other Nordic and Baltic stations and other coastal sites (e.g. MHD and FKL) and amongst the highest in Europe. Kecorius et al. (2016) have shown that ship emissions in the Baltic Sea contribute strongly to pollution levels at PLA and that up to 50% of particles arriving at PLA are generated by processes and emissions, including shipping, taking place in areas upwind the station. Moreover, Asmi et al. (2011) presented some similarities in particle number concentrations measured at PLA with those measured at some central European sites such as IPR due to the influence from multiple source

areas (cf. Fig. 3). It should be noted however, that the period with available σ_{sp} measurements is very short at PLA (cf. Table 1 and Figure 7) and the data coverage is also low (cf. Table S3). Consequently, more measurements at this site are needed in order to confirm the σ_{sp} values reported here. The other two coastal stations (MHD and FKL) register median σ_{sp} values in the upper range of σ_{sp} measured across the network mostly due to the contribution of marine aerosol in winter and mineral dust in summer at MHD and FKL, respectively (cf. Paragraph 3.5).

3.2 Variability of SAE

Figure 4 shows the box-and-whiskers plots of SAE calculated at the different stations. Table S5 and Figure S3 in the Supplementary Material report the statistics of SAE and frequency and cumulative frequency distributions, respectively. It should be noted that the comparison of SAE among the different stations could be slightly biased by the different particle size cuts upstream the integrating nephelometers used in this work (cf. Table 1). Currently, all ACTRIS integrating nephelometers measure whole air or PM_{10}. Whole air is currently measured at mountain sites (BEO, CMN, JFJ, PUY, CHC) and one coastal (MHD), and two urban/suburban (UGR and SIR) observatories (cf. Table 1). At some stations, the inlet was changed from whole air to PM_{10} at a given time, namely at OPE, FKL, and TRL. Given the lower scattering efficiency of aerosol particles larger than 10 μm, no important differences in the SAE should be expected between aerosol particles sampled with whole air and PM_{10} cut-off. At other stations the inlet was changed during the measurement period from a cut-off lower than 10 μm (1 μm at KPS; 2.5 μm or 5 μm at PAL, MSA and MAD) to PM_{10}. For PAL (where a median SAE of around 1.8 was measured; cf. Table S5), Lihavainen et al. (2015a) assumed that the inlet changes (from PM_5 to $PM_{2.5}$ in 2005 and from $PM_{2.5}$ to PM_{10}, cf. Table 1) had only minor effects on scattering, because the number concentration of coarse particles is very low at PAL. Similarly, KPS observatory registers among the highest SAE observed in the network (median value around 2) suggesting an aerosol particle size distribution dominated by fine particles. Consequently, the inlet change from PM_1 to PM_{10} at KPS had probably a minor effect on SAE. Finally, two stations (MSA and MAD) changed the inlet from $PM_{2.5}$ diameter cut-off to PM_{10}. For these two Southern European stations the inlet change may have had an effect on SAE especially during Saharan dust outbreaks, which are however sporadic events. Thus, despite the differences in the particle diameter cut-off the comparison between the different stations in terms of SAE seems feasible.

The SAE shows a huge variability across the geographical sectors (Fig. 4). On average, the highest median SAE, around 1.8 – 2.0, are observed at all central and eastern European observatories (cf. Table S5). These values are quite high indicating clearly the predominance of fine particles at these two geographical locations. Moreover, high $PM_{2.5}/PM_{10}$ ratios, indicative of presence of small particles, are typical for rural lowland sites in central Europe (e.g. Spindler et al., 2010; EMEP, 2008). Figure S3 also shows that at central and eastern sites the SAE data have very similar unimodal delta-like distributions. Exceptions are CMN, JFJ and BEO mountain sites,

where left-tailed distributions of SAE are observed likely due to the reduced effect of fine particles from the PBL in winter and an increase in the relative importance of coarse mineral dust or sea salt particles as well as aged aerosols compared to lower altitude stations in the same geographical sector.

On average, the SAE is lower at all other geographical sectors compared to central and eastern Europe even though some exceptions are observed. For example, at CBW (western Europe) the median SAE reaches values around 2.1. Indeed, both polluted air masses from industrialized zones of the Benelux countries and clean air masses from the sea contribute to the presence of aerosol particles at this site (Crumeyrolle, et al., 2010). Moreover, CBW is surrounded by several large cities at a distance of about 20 to 40 km from the station, which may have contributed to the high SAE measured in this geographical location. Asmi et al. (2011) have also shown that background particle number concentrations at CBW are much higher than for example at BIR. Median SAE close to one or lower, indicative of the fact that σ_{sp} is dominated by large particles, are observed at more remote sites such as MHD, IZO, ZEP, and TRL. Low SAE at MHD was already reported by Vaishya et al. (2011, 2012) and justified by the frequent presence mainly in winter of coarse mode sea-salt particles, since mineral dust particles can be ruled out. In fact, air masses originating from dust sources are not frequent at these sites. Similarly, the low SAE observed at ZEP and TRL can be associated with the presence of coarse sea-salt particles. Conversely, the SAE obtained at IZO is mainly due to the frequent presence of mineral dust particles from African deserts (e.g. Rodríguez et al., 2011). Very similar bi-modal frequency distributions are observed at MHD and IZO showing a pronounced left peak indicating the high probability of measuring coarse particles at these sites. BIR and PLA also show an enhanced left peak in the SAE frequency distributions.

Differently from σ_{sp}, the SAE does not show any clear gradient when moving from mountain to regional/urban sites. For example, at mountain sites the median SAE ranges between around 0.7 at IZO to values higher than two at JFJ and CMN. As reported by Zieger et al. (2012) a SAE value around 2 prevails for most of the time at JFJ and can be regarded as the typical background under non-dusty conditions. Thus, the SAE values at JFJ and CMN can be considered as representative of central Europe free troposphere and especially in winter when the PBL emissions at these sites are reduced. This high variability of SAE at mountain sites was also reported by Andrews et al. (2011). Andrews et al. (2011) reported SAE values from 11 mountaintop stations worldwide ranging from less than one to more than two. Moreover, Bourcier et al. (2012) have shown that at mountain sites coarse particles are transported more efficiently at high altitude by higher wind speed thus probably also contributing to the observed variability of SAE at mountain sites. Also at coastal sites (PLA and MHD), the SAE shows large variability with higher SAE measured at PLA compared to MHD confirming a higher effect of anthropogenic emissions at PLA compared to MHD. Less variability in median SAE is on average observed at regional sites, with the exception of OPE where a lower SAE is observed probably due to the influence of agricultural practices in the vicinity. Among the urban sites, MAD registers the lowest median SAE (1.47) compared to UGR

(1.69) and DEM (1.60). The lower SAE at MAD could be explained, as already noted, by the reduced formation of secondary inorganic aerosols during the available measurement period. Moreover, resuspended dust from vehicles could also explain the lower SAE observed at MAD observatory.

3.3 Variability of *g*

The asymmetry parameter is widely used in radiative transfer models because it provides information about how much radiation is scattered back compared to the amount of radiation scattered in the forward direction. Figure 5 shows the box-and-whiskers plots of *g* calculated at the different stations. Table S6 and Figure S4 in the Supporting Material report the statistics of *g* and frequency and cumulative frequency distributions, respectively. Given that *g* is calculated from BF using Equation 2 (Section 2.2.3), we report in Figure S5 in the Supporting material the box-and-whiskers plots of BF whereas Table S7 reports the statistics of BF. Figure 5 and Figure S5 are symmetrical, thus the lower BF the higher is *g*. As already observed for SAE, the *g* varies considerably among the different stations ranging between median values around 0.49 (CMN) to around 0.7 (TRL). Higher *g* median values are in some cases observed at mountain sites compared to regional or urban environments. This is the case for example for IZO compared to MSY, UGR and MAD in the southwestern European sector or HPB and JFJ compared to IPR, MPZ and KOS in central Europe. However, exceptions are observed for example for CMN where the median *g* value (only 2 years available) is the lowest in the central European sector and among the lowest observed in this study. On average, *g* values range between 0.49 to 0.64 at mountain sites with a mean value of 0.58±0.05. This value is consistent with the mean value of 0.61±0.05 reported by Andrews et al. (2011) at the mountain sites included in their work. Figure S6 in the Supporting material reports the mean SAE (ordered from low to high values in each geographical location) and *g* at each station used in this work and the SAE-*g* scatter plot. Figure S6 shows that no clear relationship between *g* and SAE can be observed. For example, TRL and MHD observatories register among the highest *g* observed in the network which is consistent with the very low SAE measured at these stations because of the frequent presence of coarse mode sea-salt particles (cf. Fig. 4). However, *g* values similar to TRL and MHD are also observed at stations such as PLA, BIR, JFJ, and DEM, which are dominated on average by fine aerosol particles (SAE similar or higher than 1.5). However, there are geographical locations (e.g. Nordic and Baltic, western and southwestern Europe) where SAE increases and correspondingly the *g* decreases from one station to another indicating a shift toward finer particles. However, this is not a general rule. In fact, the same relationship is not observed for example in central or eastern Europe (cf. Fig. S6). Differences in the shape of the particle number size distribution, particle shape and chemical composition (e.g. refractive index, RI) are factors likely contributing to explain the poor relationship observed between *g* and SAE. The Mie theory of polydisperse spherical particles predicts that BF is lower and *g* correspondingly higher for coarse mode aerosol particles (for which the SAE will be low) compared to fine mode particles. However, some studies deploying integrating nephelometer

have found that BF can be higher for coarse mode aerosol particles (such as mineral dust) than for fine mode aerosol particles (Carrico et al., 2003; Doherty et al., 2005). Doherty et al. (2005) suggested that an under-correction for the σ_{sp} truncation of the forward-scattered radiation (which is relatively larger for coarse particles) could bias the calculated BF high. Moreover, the shape of particle number size distribution is another factor affecting BF and SAE. Thus, differences in the relative fractions of the fine and coarse modes could also drive the BF-SAE relationship. In fact, the SAE is most sensitive to the presence of coarse mode aerosol particles compared to BF which is most sensitive to small accumulation mode particles (Delene and Ogren, 2002; Collaud Coen et al., 2007). Thus, depending on the shape of the particle number size distribution, BF and SAE might or might not correlate. Moreover, the refractive index (RI), which is strongly related to the chemical composition of the particles, is another important variable, that can affect *g* (e.g. Marshall et al., 1995). In the work from Hansen and Travis (1974; Fig. 12) the authors showed that for a given particle diameter the *g* parameter did non linearly decreased with increasing real RI. Thus, coarse mode particles with a given RI could have an asymmetry parameter similar or lower to that of fine particles with lower RI. Recently, Obiso et al. (2017) confirmed the findings by Hansen and Travis (1974) showing also that a perturbation in RI of 20% has a higher effect on *g* compared to similar relative perturbation of particle shape. On the other side, Obiso et al. (2017) showed that a variation of RI for coarse particles can have a small effect on the mass scattering efficiency of the particle and its spectral dependence and consequently on SAE.

3.4 Relationships between σ_{sp} and intensive optical properties

Figure 6 shows the relationships between σ_{sp} and SAE and between σ_{sp} and *g* at each station. Mean SAE and *g* are calculated for each σ_{sp} bin and the bin size at each station is calculated following the Freedman – Diaconis rule:

$$\text{Bin size} = 2\frac{IQR(x)}{\sqrt[3]{n}} \qquad \text{(Eq. 3)}$$

where IQR(x) is the interquartile range of the data and *n* is the number of observations in the sample *x*. This kind of graphs helps in understanding which aerosol type on average dominates the particle light scattering, depending on the amount of scattering measured. It should be noted that in Figure 6 the number of samples available at each station is not evenly distributed among the considered bins. Figure S7 in the Supplementary Material shows for some stations the SAE-σ_{sp} pairs colored by the number of samples in each bin to highlight how samples are distributed among the bins.

3.4.1 *g*-σ_{sp} relationships

The asymmetry parameter *g* shows the lowest values under very low σ_{sp} suggesting the predominance of small fine mode particles. Andrews et al. (2011) reported similar *g*-σ_{sp}

relationships at different mountain sites and suggested that the removal of large particles by cloud scavenging or by deposition during transport could explain the observed low *g* under a clean atmosphere. They also suggested that the formation of new particles followed by condensation/coagulation could generate small but optically active particles. Here, we show that this behavior of BF or *g* as a function of σ_{sp} was observed at all sites, not only at mountain sites.

The parameter *g* then increases with increasing σ_{sp} indicating a shift of the particle number size distribution towards the larger end of the accumulation mode. Delene and Ogren (2002), Andrews et al. (2011) and Pandolfi et al. (2014) showed that BF tends to decrease with increasing aerosol loading, consistent with the observed increase of *g*. For comparison with previous works, Figure S8 in the Supplementary Material shows the BF-σ_{sp} relationships for all observatories evidencing the aforementioned BF decrease with increasing σ_{sp}.

The shift of the particle number size distribution towards the large end of the fine mode with increasing σ_{sp} is probably the main reason causing the observed increase of *g* (and the decrease of BF, cf. Fig. S8). A possible explanation for this shift could be a progressive aging of atmospheric aerosol particles. Then, at the majority of stations, the variation of *g* is less pronounced under periods of high particle mass concentrations suggesting changes mostly in the coarse aerosol particles mode rather than in the fine mode.

3.4.1 SAE-σ_{sp} relationships

As reported in Figure 6, at some stations the SAE progressively increases with σ_{sp} in the σ_{sp} range where the *g* parameter increases as well. The increase of both *g* and SAE with σ_{sp}, observed for example at the Nordic and Baltic, central and eastern European observatories, could be related to the different effects that different particle sizes have on SAE and *g*. A progressive increase of SAE with σ_{sp} would suggest an increasing relative importance of fine aerosol particles. The origin of these fine particles is probably different depending on the location of the measuring site. For the remote PAL site, for example, Lihavainen et al. (2015b) observed an increase of both σ_{sp} and SAE with increasing temperature due to increasing formation of BSOA (biogenic secondary organic aerosols) with increasing ambient temperatures, thus likely driving the σ_{sp}-SAE relationships reported in Fig. 6 for PAL. The BSOA from gas-to-particle formation over regions substantially lacking in anthropogenic aerosol sources such as the European boreal region (Tunved et al., 2006) are probably strongly contributing to the σ_{sp}-SAE relationships observed at other Nordic and Baltic sites such as SMR. At polluted sites such as those located in central and eastern Europe the anthropogenic aerosol emission and the active secondary aerosol production in the region (e.g. Ma et al., 2014) are probably driven the σ_{sp}-SAE relationships reported in Fig. 6. For higher σ_{sp}, the σ_{sp}-SAE relationships changed and a progressive shift toward relatively larger particles is on average observed with increasing σ_{sp}. However, at the majority of northwestern, central and eastern European stations, the SAE keeps values around or higher 1.5 under high particle load indicating that high σ_{sp} is dominated by fine particles. An exception is MHD where SAE increases

with increasing σ_{sp} keeping values on average lower than 1.4 under high particle load (cf. Fig. 6). As already observed, low SAE at MHD is mainly due to the predominance of sea-salt coarse particles at this site (Vaishya et al., 2011). Conversely, at some sites in South Europe (e.g. MSA, MSY, IZO, DEM) the SAE reaches values around one or lower under high particle load indicating that at these stations high σ_{sp} is dominated by mineral dust coarse particles mainly from African deserts. Exceptions are two urban sites in Southwestern Europe (UGR and MAD) where fine particle likely mostly from traffic (and also from biomass burning at UGR) on average dominate the highest measured σ_{sp}. Similar σ_{sp}-SAE relationships, as those reported in Fig. 6, were observed by Andrews et al. (2011) at mountain sites and by Delene and Ogren (2002) at marine sites. Among the lowest SAE are observed at IZO, the station closest to the African continent. Interestingly, at IZO the SAE shows the highest gradient for σ_{sp} coefficients in the range of 0-50 Mm^{-1} whereas the gradient is much lower for σ_{sp} higher than 50 Mm^{-1} being the SAE almost constant for σ_{sp} higher than 100 Mm^{-1}. IZO station is often in the free troposphere and high loading at this station are only registered under Saharan dust events, thus almost only mineral dust is measured at IZO. Normally the long-rang transport mineral dust particle don't have a significant fraction above 10 µm because of the short lifetime, thus likely explaining the constant SAE observed at IZO under high aerosol loading.

3.5 Seasonal variability

Figures 7, 8 and 9 present the annual cycles of σ_{sp}, SAE and *g*, respectively, at each site. Overall, strong seasonal cycles of σ_{sp} and intensive aerosol particle optical parameters are observed at the majority of the stations even if exceptions are observed. Given the important role that the station placement plays in the seasonal cycles of aerosol parameters, the analysis is presented below separately for mountain observatories ad for low altitude observatories.

3.5.1 Seasonal variability at mountain observatories

At the mountain stations (PUY, HPB, JFJ, CMN, BEO, MSA, and IZO), σ_{sp} peaks in spring/summer whereas lower σ_{sp} values are measured in autumn/winter. Similar findings were for example already reported by Nyeki et al. (1998) for JFJ and summarized by Andrews et al. (2011) for many mountain top stations worldwide and by Pandolfi et al. (2014) for MSA station. Different factors contribute to the σ_{sp} increase in spring/summer at the mountaintop observatories, such as the increase of the boundary layer height and stronger upslope winds during the warmest months. Moreover, specific events such as Saharan mineral dust outbreaks, may contribute to the increased σ_{sp} observed at mountain stations in spring/summer, and especially in southern Europe (e.g. Pey et al., 2013; Pandolfi et al., 2014; Rodríguez et al., 2011). At IZO, σ_{sp} peaks strongly in July-August because of the very high influence of African mineral dust at this station during these

months (e.g. Alastuey et al., 2005; Diaz et al., 2006). At the mountaintop CHC observatory, σ_{sp} progressively increases during the dry season, from May to October, reaching lower values during the rainy season (from December to April). Moreover, during the dry season the new particle formation events, taking place at CHC with one of the highest frequency reported in the literature so far (Rose et al. 2015), can introduce very small particles that grow to the nucleation and Aitken mode. At the mountain stations, both SAE and σ_{sp} are on average higher in summer compared to the winter period, thus suggesting a higher anthropogenic influence at these sites during the warmest months. The summer SAE increase is more evident at some mountain stations, e.*g*. HPB, CMN, and BEO, compared to other mountain stations such as JFJ and MSA. Less pronounced SAE seasonal variation at JFJ was related by Bukowiecki et al. (2016) to the rather constant composition of the JFJ aerosol. At the southern station of MSA the observed less pronounced seasonal cycle of SAE could be related with the Saharan dust outbreaks which contrast the PBL transport of fine particles observed at other mountain sites. At IZO, the SAE reaches the lowest values during July-August being the Saharan dust outbreaks very intense at this site during this period.

Overall, the *g* parameter shows opposite seasonal cycles compared to SAE at almost all mountain stations with the exception of JFJ and BEO where *g* slightly increases with SAE in summer. At almost all mountain stations, the seasonal variations of SAE and *g* are less pronounced compared to the seasonal variation of σ_{sp} indicating larger seasonal variation in the extensive aerosol optical properties than in the intensive properties. For example, the median σ_{sp} values at MSA increase by around 800% during summer (JJA) compared to winter (DJF), whereas SAE and *g* increase by around 5-7%. Similar relative increases are observed at JFJ (660%, 16% and 11% for σ_{sp}, SAE and *g*, respectively) whereas the relative increases are much higher at BEO, especially for σ_{sp} (around 1300%) and SAE (26%). At CMN, the median σ_{sp} value increases by around 400% from winter to summer, whereas SAE and *g* increase and decrease, respectively, by around 46% and 6%, respectively. At CHC, the SAE decreases as the σ_{sp} increases moving from wet to dry season, indicating an increasing effect of coarse particles on σ_{sp} during the dry season. At PUY, σ_{sp} peaks from March to September and this increase is accompanied by a small SAE increase. Venzac et al. (2009) and Boulon et al. (2011) have shown that PUY is more often influenced by the free troposphere or residual layers in winter and spring compared to the summer season.

3.5.1 Seasonal variability at low altitude observatories

At some of the low altitude observatories, the seasonal variation of particle scattering is opposite compared to the variations observed at mountain sites, σ_{sp} being higher in winter and lower in summer. MHD, CBW and SIR in the western sector, IPR, MPZ and KOS in central, KPS in eastern and UGR in south-western Europe show such increase in particle mass concentration in wintertime. The reasons causing these marked seasonal cycles are probably different depending on the geographical sector considered.

3.5.1.1 Central and eastern Europe

Central and eastern European observatories show marked seasonal cycles of both extensive and intensive aerosol particles optical properties. In these regions, less horizontal and vertical pollutant dispersion in winter, due to a higher frequency of stagnant conditions and temperature inversions, play an important role in accumulating aerosols. As a consequence, as reported in Figure 7, the σ_{sp} is much higher in winter compared to summer. SAE and *g* also show marked season cycles in these regions, being the SAE (*g*) higher (lower) in summer compared to winter (cf. Fig. 8). Ma et al. (2014) have shown that at MPZ an increased SAE in summer is mainly explained by the variation of the particle number size distribution. Thus, high concentrations in spring and summer of small particles during new particle formation and subsequent growth cause the observed increase of SAE during warmest months.

3.5.1.2 Nordic and Baltic regions

At the Nordic and Baltic sites, the monthly variation of σ_{sp} is on average less pronounced compared to the central or eastern European stations and especially at BIR, SMR and PAL. This is likely due to the placement of these stations located in remote areas with different meteorology (e.g. less pronounced PBL variations) and where on average much lower σ_{sp} values are measured compared to other European sites. Moreover, this could also indicate the importance of anthropogenic sources like domestic heating in central and eastern Europe in winter. However, the monthly variation of SAE and *g* is rather pronounced at these Nordic and Baltic observatories: SAE (*g*) increases (decreased) in summer compared to winter indicating the predominance of relatively smaller particles during the warmest months. Similar findings were reported for the SMR and PAL observatories by Virkkula et al. (2011) and Lihavainen et al. (2015a), respectively. The observed seasonal variations in intensive aerosol optical properties were related to both the transport of different air masses at these remote sites depending on the season and the enhanced formation of BSOA in summer (e.g. Lihavainen et al., 2015a). Lihavainen et al. (2015a) and Virkkula et al. (2011) also reported a lower single scattering albedo in winter compared to summer at PAL and SMR, respectively, frequently dropping below 0.7 at SMR due to a significant contribution from light absorbing carbon, mostly from residential wood combustion. Thus, they have shown that aerosol particles observed in summer at SMR and PAL had the potential to cool the atmosphere more efficiently than those observed during winter. Similar intensive optical properties season cycles were observed at BIR.

3.5.1.3 Western Europe

Similarly to the Nordic and Baltic regions, differences in aerosol sources and sinks are the likely reasons explaining the seasonal variation of σ_{sp}, SAE and *g* observed in western Europe. Marked σ_{sp} seasonal cycles are observed at all low altitude western European observatories, with higher values measured in winter compared to summer. On average, at these sites, SAE (*g*) is higher (lower) in summer compared to winter. O'Connor et al. (2008) and Vaishya et al. (2011, 2012)

showed that the background marine aerosol measured at MHD contains a strong and significant seasonal cycle with sea-salt dominating in winter and biogenic organic aerosol dominating the submicron sizes in summer. This is consistent with the observed season cycles of SAE and *g* reported here for MHD.

3.5.1.4 South Europe

Among the southern European observatories, marked seasonal variation for σ_{sp} is observed especially at UGR, MSY and FKL. At the urban UGR site, the mean aerosol type is very different in winter compared to summer. As evidenced by the seasonal cycles of SAE and g, aerosol particles are generally finer in winter at UGR compared to the summer season as already observed for example by Lyamani et al. (2010; 2012) and Titos et al. (2012). This is likely due to the accumulation of fine particles, mainly from traffic, domestic heating and biomass burning, favored by stagnant conditions and atmospheric inversions during winter. In summer, the higher frequency of Saharan mineral dust outbreaks at this site increases the mean size of the particles during the warmest months. At the MSY regional site, the higher efficiency of the sea breeze in transporting pollutants from the urbanized/industrialized coastline toward regional inland areas during the warmer season mainly explains the summer increase in aerosol particle mass concentration observed at this site (e.g. Pandolfi et al., 2011). Moreover, the enhanced formation of secondary sulfate and organic matter in summer together with frequent Saharan mineral dust outbreaks, strongly contribute to the observed seasonal cycle for σ_{sp} and intensive properties at MSY site. The σ_{sp} peak observed at MSY in March is due to the winter pollution episodes typical of the western Mediterranean basin (WMB) (e.g. Pandolfi et al., 2014a and references therein). During these episodes, the accumulation of pollutants close to the emission sources is favored by anticyclonic conditions coupled with strong atmospheric inversions. During such conditions, pollutants accumulate in the PBL and can subsequently reach the station when PBL height increases. On average, at MSY low SAE are measured in April and October likely due to the occurrence of Saharan dust outbreaks during these months. At FKL no intensive optical aerosol properties are available. The high σ_{sp} in summer at this site is also associated with mineral dust storm events as for example reported by Vrekoussis et al. (2005). However, mineral dust storms in the Mediterranean are not the only reason for the observed increased σ_{sp} in summer. In fact, as for example reported by Kalivitis et al. (2011) for FKL and Pandolfi et al. (2011) for MSY, ammonium sulfate and particulate organic matter, whose concentrations increase in summer in the Mediterranean Basin, were assumed as important contributors to σ_{sp} during the warm season. At the DEM urban observatories, the high σ_{sp} measured in spring are linked to Saharan dust outbreaks as also supported by the seasonal cycles of SAE and *g* which showed the lowest and highest, respectively, values in spring.

3.6 Trends

Trends of σ_{sp}, SAE and BF are studied for those stations having more than 8 years of data (13 observatories). Generally, it is recommended to have more than 10 years of data for trend studies. Among the ACTRIS stations, PAL, SMR, MHD, HPB, IPR, JFJ, and UGR have more than 10 yr of data, whereas at PUY, MPZ, CMN, BEO, KPS, and IZO, 8 or 9 years are available. These stations are included in order to improve the spatial coverage, similarly as in Collaud Coen et al. (2013). The Theil Sen statistical estimator (Theil, 1950; Sen, 1968) is used here to determine the regression parameters of the data trends, including slope, uncertainty in the slope and p-value. The Theil Sen method provides similar results as the Mann-Kendall test and it is implemented for example in the Openair Package available for R space (Carslaw, 2012; Carslaw and Ropkins, 2012). The applied method yields accurate confidence intervals even with non-normal data and it is less sensitive to outliers and missing values (Hollander and Wolfe, 1999). Monthly means are used for trend analysis and the data are deseasonalized. The data coverage of σ_{sp} is higher than 70% at all stations included in trend analyses with the exception of IZO where the σ_{sp} data coverage is 55%. For SAE, the data coverage is higher than 65% at all sites with the exception of PAL (54%), PUY (59%), and IZO (52%). For BF, the data coverage is higher than 65% with the exception of PAL (26%), PUY (43%), BEO (47%) and IZO (27%). At the remote (PAL) or mountain stations (PUY, BEO, and IZO), the percentage for the intensive aerosol particle optical properties is lower because of a higher probability of measuring σ_{sp} lower than the threshold (0.8 Mm^{-1}) selected for the calculation of SAE and BF. Table 2 reports the trends observed for σ_{sp}, SAE and BF at the thirteen observatories included in this analysis. Magnitude and statistical significance of the trends for these parameters are reported in Table S8 in the Supporting Material. It should be noted that changes in particle size cut-off reported for PAL and KPS (cf. Table 1) may have affected the reported trend analyses at these stations, but estimating the impact of these changes in the observed trend is not simple. However, as already noted, Lihavainen et al. (2015a) reported that at PAL the inlet changes had minor effects on scattering, because the number concentration of coarse particles is very low at this observatory. KPS is dominated by very fine particles and the change from PM_1 to PM_{10} had probably a minor effect on σ_{sp}, SAE and BF. Moreover, at KPS the inlet was changed in April 2008, less 1.5 years after the beginning of the measurements thus likely having a minor effect in the trend analysis performed at this site over the period 2006 – 2014. The FKL observatory was removed from trend analysis because the inlet was changed from whole air to PM_{10} in 2009, from PM_{10} to PM_1 in 2011, and again from PM_1 to PM_{10} in 2013 (cf. Table 1), thus likely having a major effect on the measured particle optical properties.

In Table 2, a comparison with previous trends analysis results presented by Collaud Coen et al. (2013) for aerosol particle optical properties and by Asmi et al. (2013) for particle number concentrations is also reported.

Atmos. Chem. Phys. Discuss., https://doi.org/10.5194/acp-2017-826
Manuscript under review for journal Atmos. Chem. Phys.
Discussion started: 13 October 2017

3.6.1 Trends of σ_{sp}

Overall, σ_{sp} decreases at the majority of the stations included in this work. Significantly decreasing trends for σ_{sp} are observed at: the two Nordic and Baltic observatories (PAL for the period 2000 – 2010 and SMR); at two observatories (HPB and IPR) out of five observatories in central Europe; and at the two observatories in southwestern Europe (IZO and UGR). The trends are not statistically significant in western (MHD and PUY) and eastern (BEO and KPS) Europe. The highest magnitude of σ_{sp} trend [Mm^{-1}/yr] (cf. Table S8 in the Supplementary Material) is observed at the polluted IPR observatory. Conversely, the lowest magnitude is observed at the remote PAL observatory. For the periods considered in this work, the total reductions (TR) for σ_{sp} range between around 30% (SMR) and 60% (IZO). The high TR observed at IZO might be affected by the intensity and frequency of Saharan dust outbreaks at this site. However, estimating the effects of these events at IZO is beyond the scope of this study. Overall, the observed decreasing trends of σ_{sp} are consistent with the uniform decrease in aerosol optical depth observed in Europe (AERONET data in Li et al., 2014). A statistically significant decreasing trend of σ_{sp} at IPR was also reported by Putaud et al. (2014) for the period 2002 – 2010. As reported in Table 2 statistically significant decreasing trend for σ_{sp} is observed at around 50% of the stations considered here. Overall, the observed statistically significant decreasing trends of σ_{sp} are consistent with the demonstrated reduction of PM concentration in the atmosphere in Europe in these last decades thanks to the implementation of European/national/regional/local mitigation strategies. These decreasing trends are also consistent with trends of aerosol chemistry derived from observations in urban environments in Europe (e.g. EEA, 2013; Barmpadimos et al., 2011; Titos et al., 2014; Pandolfi et al., 2016), regional and remote environments in western Mediterranean (Cusack et al., 2012; Pandolfi et al., 2016) and in general with derivation of trends for aerosol chemistry across Europe (Tørseth et al., 2012). Recently, Collaud Coen et al. (2013) showed that trends in σ_{sp} are observed at most of the US continental sites and that these trends are generally consistent with the strong SO_2 and PM reductions observed in the US (Asmi et al., 2013; EPA, 2011). Conversely, in Europe the strong decreasing trend observed for SO_2 (e.g. Tørseth et al., 2012; Henschel et al., 2013) and, with a lower spatial homogeneity and statistical significance, for $PM_{2.5}$ (e.g. EEA, 2016) is not observed for aerosol optical properties. As reported in Collaud Coen et al. (2013) the reasons why at some of the European sites no significant trends are observed, might be related to the spatial inhomogeneities and under-representation of continental Europe PBL sites (e.g. Laj et al., 2009) and/or the timing of the SO_2 and PM trends for the US and Europe. In Europe the emissions reductions were greater for the period 1980–2000 compared to the period 2000 – 2010 (e.g. Colette et al., 2016; Tørseth et al., 2012; Manktelow et al., 2007), thus the measurements of optical particle properties in Europe may not go back far enough to reflect the time period with the largest emission reductions. Tørseth et al. (2012) reported average reductions for ambient sulfate and nitrate mass concentrations in Europe of -12% and -1%, respectively, during 2000 – 2009 compared to -24% and -7%, respectively, during 1990 – 2000. They also reported statistically

significant decreases of PM_{10} and $PM_{2.5}$ mass concentrations at around 50% of European sites with total reductions of -18% and -27%, for PM_{10} (24 sites) and $PM_{2.5}$ (13 sites), respectively, during 2000 – 2009. A direct comparison between the stations included in this work and those included in Tørseth et al. (2012) is not possible because of the different timing of reported σ_{sp} and PM mass concentration measurements. At those stations where a significant decreasing trend for σ_{sp} is observed and considering a period of 10 yr (even if not coincident for all stations), the total reduction for σ_{sp} in Europe is around -35% (cf. Table S8) consistent with the trend reported by Tørseth et al. (2012) for PM in Europe. Quite good agreement, even though again likely biased by the different timings, is also observed comparing PM mass concentration and σ_{sp} trends by geographical sectors. A significant total reduction around -40 ÷ -30% was reported for PM_{10} and $PM_{2.5}$ in the Nordic and Baltic sector by Tørseth et al. (2012; cf. Fig. 7 in Tørseth et al. (2012)) in close agreement with the statistically significant total decrease of σ_{sp} around -34% reported for PAL during 2000 – 2010 (cf. Table S8). In the Western sector (MHD) the decreasing trend for $PM_{2.5}$ during 2000 – 2009 was insignificant (-10 ÷ 0%) as reported here for σ_{sp} during the period 2001 – 2010. In the Central sector statistically significant decreases for $PM_{2.5}$ and PM_{10} mass concentrations ranged between -20% and -40% during a 10 yr period (2000 – 2009) and the total reduction for σ_{sp} ranged between -38% (HPB) and around -48% (IPR). In the Southwestern European sector the total reduction for σ_{sp} is around -32% (at UGR) and -60% (at IZO), whereas Tørseth et al. (2012) reported around -20 ÷ -40% decrease for the PM10 mass concentration. To further confirm the observed close agreement between PM trends reported in literature and the trends of σ_{sp} in this work, Table S9 in the Supporting Material reports the comparison between σ_{sp} and PM_{10} and/or $PM_{2.5}$ mass concentration trends calculated at those stations where simultaneous σ_{sp} and PM mass concentration measurements are available. As reported in Table S9 both the observed total reductions and the statistical significance of the trends are very similar for σ_{sp} and PM_{10}.

3.6.2 Trends of SAE and BF

The trends for SAE are estimated for three different quantities, namely: the SAE calculated as linear fit using three wavelengths (b-g-r), using the blue and the green wavelengths (b-g) and using the green and red wavelengths (g-r). For the periods considered in this work (in bold in Table 2), the SAE calculated using the three wavelengths (b-g-r) shows statistically significant trends at five sites. At PAL (Nordic and Baltic), PUY (western Europe) and BEO (eastern Europe) decreasing trends are observed, whereas increasing trends are observed at HPB (central Europe) and UGR (southwestern Europe). Uniform negative trends of columnar Ångström exponent from AERONET data were reported by Li et al. (2014) across Europe and these trends were ascribed to reduced fine-mode anthropogenic emission. The positive SAE trend observed at HPB and UGR would suggest a shift of the accumulation mode particles towards smaller sizes and/or a change in the

coarse aerosol mode. For example, the SAE increase at UGR could be probably explained by a progressive relative importance of fine particles emissions driven by a progressive reduction of coarse particles for example from construction/demolition works due to the economic crisis which affected Spain from 2008 (e.g. Lyamani et al., 2011; Querol et al., 2014; Pandolfi et al., 2016). In fact, Titos et al. (2014) reported statistically significant decreasing trend for PM_{10} fraction during the period 2006 – 2010 whereas no trend was observed for PM_1 fraction. Moreover, at UGR, statistically significant increasing trend is also observed for the SAE calculated using the green and red wavelengths (g-r), likely more sensitive to the coarser particle mode, whereas the trend was non-statistically significant for the SAE b-g. The possible change in the coarse aerosol mode at UGR is likely also causing the observed statistically significant increasing trend of BF (cf. Table 2), given that a positive trend of BF would be consistent with a shift of the accumulation mode particles towards smaller sizes. Similarly, statistically significant increasing trends for both SAE and BF are also observed at SMR (SAE b-g) and HPB. Statistically significant increasing trends of BF are also observed at the other Nordic and Baltic stations (PAL) and at PUY (western Europe), where the SAE shows statistically significant decreasing trends, and at IPR (central Europe) where the trend of SAE was insignificant. Thus, overall, the trends of BF are positive at all stations where BF measurements are available. The opposite sign of the trends of SAE and BF at PAL and PUY could be due to different effects that different particle sizes have on SAE and *g* or a progressive change in the mean diameter of the fine mode aerosol. Further research involving for example size distribution data and Mie calculation could help in understanding the differences observed in some cases between SAE and BF (or *g*). Recently, Korras-Carraca et al. (2015) have shown that the column integrated *g* from Modis-Terra had widely statistically significant positive trends (2002-2010) with stronger increases observed in the eastern and southern Black Sea, as well as over the Baltic and Barents seas. Moreover, both Modis-Terra and Modis-Aqua produce positive trends of *g* in the eastern Mediterranean Sea and the eastern coast of the Iberian Peninsula. Positive trends for *g* would correspond to negative trends for BF. The difference observed with our work could be due to the different variability often observed between near-surface measurements and column integrated measurements which can confound the relationship between surface and column optical properties (e.g. Bergin et al., 2000; Lyamani et al., 2010). Although, it was shown that mid altitude station might be globally representative of the whole atmopheric column (Chauvigne et al., 2016).

3.6.3 Comparison with previous trend analyses

Table 2 shows the comparison, over the same periods, between the trend analyses performed in this work and the analyses presented by Collaud Coen et al. (2013) for aerosol particle optical properties and by Asmi et al. (2013) for particle number concentrations ($N_{LDL-500}$, N_{20-500} and $N_{100-500}$). An agreement with the results from Collaud Coen et al. (2013) is observed for JFJ where consistent insignificant trends are detected for the three periods reported in Collaud Coen et al. (2013). For MHD, we calculated a non-significant increasing trend for σ_{sp} during 2001 – 2010,

whereas Collaud Coen et al. (2013) reported a statistically significant increasing trend for the same period. At PAL, non-statistically significant trend for σ_{sp} is observed here and in Collaud-Coen et al. (2013) for the period 2001 – 2010, whereas we observe a statistically significant decreasing trend for the period 2000 – 2010. Moreover, at PAL, we observe statistically significant decreasing trend for SAE during the two common periods which were insignificant in Collaud Coen et al. (2013). It should be noted that Collaud Coen et al. (2013) reported insignificant SAE trend at PAL using the Mann Kendall test whereas they reported statistically significant decreasing trends using the GLS/ARB and LMS methods, consistent with our work. These differences are thus likely due to the relative short period used in these trend analyses and the different sensitivity of the methods used to the presence of missing values or outliers especially at PAL where σ_{sp} is very low (cf. Fig. 2). For example, in this work the SAE calculated for PAL during the year 2007 was removed from the trend analysis due to the presence of too many extreme high SAE values, thus also likely explaining the difference observed for SAE with the work from Collaud Coen et al. (2013). Moreover, here we use de-seasonalized monthly means for trend analyses whereas Collaud-Coen et al. (2013) used de-seasonalized medians with different time granularity (3 days) thus likely affecting the comparison, especially over relatively short periods.

A comparison of trends analysis results between σ_{sp} and the particle number concentration is not straightforward as the σ_{sp} measurements are more sensitive to the particle number concentration in the upper end of the fine mode than to smaller particles. For example, Asmi et al. (2013) reported that, globally, no strong similarities were observed between σ_{sp} and N trends and that the N trends are controlled by particles in the larger range of the Aitken mode and smaller range of the accumulation mode, e.g. ca. 50–150 nm diameter. In this work, as reported in Table 2, the statistically significant decreasing trend reported for N during the period 2001 – 2010 is not observed for σ_{sp}. However, differences are also observed at PAL between N20 and N100 mainly because DMPS measurements at PAL had long gaps during periods with unusually low concentrations thus effectively removing low concentrations from the trend analysis (Asmi et al., 2013).

3.6.4 Daytime and nighttime trend analyses at mountain sites

Finally, the analysis of the trends during daytime (08:00 – 16:00 GMT) and nighttime (21:00 – 05:00 GMT) by season at mountain stations are also analyzed (Table 3). This analysis could provide information about changes in σ_{sp} when the mountain stations are likely affected by the PBL (e.g. daytime and/or summer) or by the residual layer (e.g. nighttime in summer) or when these are representative of the free troposphere (e.g. nighttime in winter). Consistently with what reported in Table 2 for σ_{sp}, the trends are insignificant at JFJ, PUY CMN, and BEO irrespective of the time of the day or season. The decreasing trends observed at HPB, also reported in Table 2, are

statistically significant only during autumn, irrespective of the time of the day. Conversely, the trend observed for σ_{sp} at IZO reported in Table 2, is not observed by splitting the analysis by time of the day and/or season.

Conclusions

This investigation presented the near-surface in-situ σ_{sp} (aerosol particle light scattering), SAE (Scattering Ångström exponent), BF (backscatter fraction), and *g* (asymmetry parameter) measurements obtained over the past decade at 28 measuring atmospheric observatories which are part of the ACTRIS Research Infrastructure and most of them belong to the GAW network. Results show a large variability of both extensive and intensive aerosol particle optical properties across the network, which is consistent with the previously reported variability observed for other aerosol particle properties such as particle mass concentration, particle number concentration and chemical composition. Main findings can be summarized as follows:

- Overall, the highest σ_{sp} are measured at low altitude observatories in central and eastern Europe and at some urban sites in south Europe whereas, the lowest σ_{sp} are observed at some mountain stations and at two Arctic and Antarctic sites. Low σ_{sp} levels, comparable with those measured at mountain sites, are also observed at the majority of the regional/continental Nordic and Baltic observatories. The σ_{sp} values in Western Europe are on average higher compared to those measured in the Nordic and Baltic regions and lower compared to those measured at regional level in south Europe. Some exceptions to these general features are however observed.
- In central and eastern Europe, independently from the station placement, the SAE *(g)* is among the highest (lowest) observed across the network indicating a large predominance of fine particles. In these regions, the SAE *(g)* is even higher (lower) in summer compared to winter suggesting the shift toward the small end of the aerosol particle size distribution likely linked to new particle formation events during the warmest months. On average SAE *(g)* is lower (higher) in the Nordic and Baltic, western and southern sectors compared to central and eastern Europe.
- Seasonal cycles for σ_{sp} are observed in all geographical sectors. These are especially marked at regional level in central and eastern Europe where wintertime episodes linked with stable air and thermal inversions favor the accumulation of pollutants. Clear annual cycles are also observed at mountain sites where σ_{sp} is higher in summer because of the enhanced boundary layer influence. In some cases, SAE (*g*) is also high (low) in summer at mountain sites indicating a higher PBL anthropogenic influence during the warmer months. In the Nordic and Baltic regions, the seasonal variation of σ_{sp} is less pronounced compared to central and eastern Europe likely due to different meteorology and less pronounced PBL variations. Despite the relatively small σ_{sp} seasonal cycles in the Nordic and Baltic regions, SAE (*g*)

increases (decreases) in these regions in summer compared to the winter period likely due to a seasonal-dependent transport of air masses at these remote sites and an enhanced formation of secondary organic aerosols previously observed at these sites during the warmest months. At coastal sites in northwestern Europe, the presence of sea-salt particles in winter also contributes to the observed pronounced seasonal cycles of SAE and *g*.

- The analysis of the systematic variability of SAE and *g* as a function aerosol loading (σ_{sp}) reveals some common patterns. At all stations, *g* shows the lowest values under very low σ_{sp} likely because the formation of new particles in a clean atmosphere followed by condensation/coagulation with consequence generation of small but optically active particles. The *g* then sharply increases with increasing σ_{sp} indicating the shift of the particle number size distribution toward the larger and of the accumulation mode. Then, under periods of high particle mass concentrations, the variation of *g* is less pronounced at the majority of the stations contrary to the SAE which increases or decreases suggesting changes mostly in the coarse aerosol particles mode rather than in the fine mode.
- The analyses of the trends reported in this investigation provide evidence that both extensive and intensive aerosol optical properties have significantly changed at some of the locations include here over the last 10 and 15 years. The σ_{sp} decreasing trends reported here are statistically significant at 5 out of 13 stations included in the analysis. These 5 stations are located in the Nordic and Baltic, central and southwestern sectors. Conversely, σ_{sp} decreasing trends are not statistically significant in western and eastern Europe. Statistically significant decreasing trends of SAE are observed at 3 out of 10 observatories included in the analysis: one site the Nordic and Baltic sector and two mountain sites in the western and eastern sectors. These negative trends could be ascribed to reduced fine mode anthropogenic emission as already observed in literature for columnar SAE in Europe. Conversely, at two stations (one mountain site in central Europe and one urban site in southwestern Europe), the SAE shows statistically significant increasing trend suggesting a shift of the accumulation mode particles towards smaller sizes and/or a change in the coarse aerosol mode. At the remaining 5 observatories the reported SAE trends are not statistically significant. The backscatter fraction shows statistically significant increasing trend at 6 out of 9 sites where BF measurements are available. At three stations (the mountain site in central Europe, the urban site in southwestern Europe and one of the two sites in the Nordic and Baltic sector), both BF and SAE increase suggesting consistent evidence of a shift of the accumulation mode particles towards smaller size. Conversely, at the other site in the Nordic and Baltic sector and at one mountain site in the western sector BF increases whereas SAE decreases.

In conclusion, this investigation provides a clear and useful picture of the spatial and temporal variability of the surface in-situ aerosol particle optical properties in Europe. The results presented here give a comprehensive view of the particle optical properties and provide a reliable analysis of aerosol optical parameters for model constraints. In addition, the analysis presented here suggests

findings that may need additional investigation. For example, the fact that at some of the stations the trend of σ_{sp} changes in terms of both statistically significance and sign depending on the period used, suggests that trend analyses are necessary in the future when longer-duration records will be available. Moreover, the fact that at some sites BF and SAE show different sign in the trends suggests that further analysis is needed to better understand how other aerosol parameters such as particle size distribution and mean diameter affect the relationships between BF and SAE.

Acknowledgments

This project has received funding from the European Union's Horizon 2020 research and innovation programme under grant agreement No 654109, ACTRIS (project No. 262254), ACTRIS-PPP (project No 739530). We also thank the International Foundation High Altitude Research Stations Jungfraujoch and Gornergrat (HFSJG), which made it possible to carry out the experiments at the High Altitude Research Station at the Jungfraujoch and the support by MeteoSwiss within the Swiss program of the Global Atmosphere Watch (GAW) of the WMO. MAD station is co-financed by the PROACLIM (CGL2014-52877-R) project. SMR station acknowledges BACCHUS (project No. 603445), CRAICC (project No. 26060) and Academy of Finland (project No. 3073314). UGR station is co-financed by the Spanish Ministry of Economy and Competitiveness through project CGL2016-81092-R. Measurements at Montseny and Montsec stations were supported by the MINECO (Spanish Ministry of Economy and Competitiveness) and FEDER funds under the PRISMA project (CGL2012-39623-C02/00), by the MAGRAMA (Spanish Ministry of Agriculture, Food and Environment) and by the Generalitat de Catalunya (AGAUR 2014 SGR33 and the DGQA). Measurements at Izaña were supported by AEROATLAN project (CGL2015-17 66229-P), co-funded by the Ministry of Economy and Competitiveness of Spain and the European Regional Development Fund. Station Košetice is supported by Ministry of Education, Youth and Sports of the Czech Republic within project for support of national research infrastructure ACTRIS – participation of the Czech Republic (ACTRIS-CZ – LM2015037). Measurements at Puy de Dôme were partly supported by CNRS-INSU, University Clermont-Auvergne, OPGC and the french CLAP program. PAL station acknowledges KONE Foundation, Academy of Finland (project No. 269095 and No. 296302). CHC station received support from Institut de Recherche pour le Développement (IRD) under both Jeune Equipe program attributed to LFA and support to ACTRIS-FR program. CHC received grants from Labex OSUG@2020 (Investissements d'avenir – ANR10 LABX56). Marco Pandolfi is funded by a Ramón y Cajal Fellowship (RYC-2013-14036) awarded by the Spanish Ministry of Economy and Competitiveness. The authors would like to express their gratitude to D. C. Carslaw and K. Ropkins for providing the OpenAir software used in this paper (Carslaw and Ropkins, 2012; Carslaw, 2012).

Bibliography

Aaltonen, V., Lihavainen, H., Kerminen, V.-M., Komppula, M., Hatakka, J., Eneroth, K., Kulmala, M., and Viisanen, Y.: Measurements of optical properties of atmospheric aerosols in Northern Finland, Atmos. Chem. Phys., 6, 1155-1164, doi:10.5194/acp-6-1155-2006, 2006.

Alastuey, A., Querol, X., Castillo, S., Escudero, M., Avila, A., Cuevas, E., Torres, C., Romero, P.-M., Exposito, F., García, O., Diaz, J. P., Van Dingenen, R., and Putaud, J. P.: Characterisation of TSP and PM2.5 at Izaña and Sta. Cruz de Tenerife (Canary Is lands, Spain) during a Saharan dust episode (July 2002), Atmos. Environ., 39, 4715–4728, doi:10.1016/j.atmosenv.2005.04.018, 2005.

Anderson, T. L. and Ogren, J. A.: Determining Aerosol Radia Radiative Properties Using the TSI 3563 Integrating Nephelometer, Aerosol Sci. Tech., 29, 57–69, 1998.

Andrews, E., Sheridan, P. J., Fiebig, M., McComiskey, A., Ogren, J. A., Arnott, P., Covert, D., Elleman, R., Gasparini, R., Collins, D., Jonsson, H., Schmid, B., and Wang, J.: Comparison of methods for deriving aerosol asymmetry parameter, J. Geophys. Res. Atmos., 111, D05S04, doi:10.1029/2004JD005734, 2006.

Andrews, E., Ogren, J. A., Bonasoni, P., Marinoni, A., Cuevas, E., Rodríguez, S., Sun, J. Y., Jaffe, D. A., Fischer, E. V., Baltensperger, U., Weingartner, E., Collaud Coen, M., Sharma, S., Macdonald, A. M., Leaitch, W. R., Lin, N.-H., Laj, P., Arsov, T., Kalapov, I., Jefferson, A., and Sheridan, P.: Climatology of aerosol radiative properties in the free troposphere, Atmos. Res., 102, 365–393, doi:10.1016/j.atmosres.2011.08.017, 2011.

Asmi, A., Wiedensohler, A., Laj, P., Fjaeraa, A.-M., Sellegri, K., Birmili, W., Weingartner, E., Baltensperger, U., Zdimal, V., Zikova, N., Putaud, J.-P., Marinoni, A., Tunved, P., Hansson, H.-C., Fiebig, M., Kivek¨as, N., Lihavainen, H., Asmi, E., Ulevicius, V., Aalto, P. P., Swietlicki, E., Kristensson, A., Mihalopoulos, N., Kalivitis, N., Kalapov, I., Kiss, G., de Leeuw, G., Henzing, B., Harrison, R. M., Beddows, D., O'Dowd, C., Jennings, S. G., Flentje, H., Weinhold, K., Meinhardt, F., Ries, L., and Kulmala, M.: Number size distributions and seasonality of submicron particles in Europe 2008–2009, Atmos. Chem. Phys., 11, 5505–5538, doi:10.5194/acp-11-5505-2011, 2011.

Asmi, A., Collaud Coen, M., Ogren, J. A., Andrews, E., Sheridan, P., Jefferson, A.,Weingartner, E., Baltensperger, U., Bukowiecki, N., Lihavainen, H., Kivek¨as, N., Asmi, E., Aalto, P. P., Kulmala, M.,Wiedensohler, A., Birmili,W., Hamed, A., O'Dowd, C., Jennings, S. G.,Weller, R., Flentje, H., Mari Fjaeraa, A., Fiebig, M., Lund Myhre, C., Hallar, A. G., Swietlicki, E., Kristensson, A., and Laj, P.: Aerosol decadal trends – Part 2: In-situ aerosol particle number concentrations at GAW and ACTRIS stations, Atmos. Chem. Phys., 13, 895–916, doi:10.5194/acp-13-895-2013, 2013.

Barmpadimos, I., Hueglin, C., Keller, J., Henne, S., and Prevot, A. S. H.: Influence of meteorology on PM10 trends and variability in Switzerland from 1991 to 2008, Atmos. Chem. Phys., 11, 1813– 1835, doi:10.5194/acp-11-1813-2011, 2011.

Barmpadimos, I., Keller, J., Oderbolz, D., Hueglin, C., and Prévôt, A. S. H.: One decade of parallel fine (PM2.5) and coarse (PM10–PM2.5) particulate matter measurements in Europe: trends and variability, Atmos. Chem. Phys., 12, 3189-3203, doi:10.5194/acp-12-3189-2012, 2012.

Bergin, M. H., Schwartz, S. E., Halthore, R. N., Ogren, J. A., and Hlavka, D. L.: Comparison of aerosol optical depth inferred from surface measurements with that determined by Sun photometry for cloud-free conditions at a continental US site, J. Geophys. Res., 105, 6807–6816, 2000.

Boulon, J., Sellegri, K., Hervo, M., and Laj, P.: Observations of nucleation of new particles in a volcanic plume, P. Natl. Acad. Sci. USA, 108, 12223–12226, doi:10.1073/pnas.1104923108, 2011.

Bourcier L., K. Sellegri, P. Chausse, J. M. Pichon and P. Laj "Seasonal variation of water-soluble inorganic component in size-segregated aerosol at the puy de Dôme station (1465 m a.s.l.), France", Journal of Atmospheric Chemistry, DOI: 10.1007/s10874-012-9229-2, 2012.

Bukowiecki, N., Weingartner, E., Gysel, M., Collaud Coen, M., Zieger, P., Herrmann, E., Steinbacher, M., Heinz, Gäggeler, W., Baltensperger, U.: A review of more than 20 years of aerosol observation at the high altitude research station Jungfraujoch, Switzerland (3580 m asl), Aerosol and Air Quality Research, 16: 764–788, doi: 10.4209/aaqr.2015.05.0305, 2016.

Carrico, C.M., Kus, P., Rood, M.J., Quinn, P.K., Bates, T.S.: Mixtures of pollution, dust, sea salt, and volcanic aerosol during ACE-Asia: radiative properties as a function of relative humidity, J. Geophys. Res., 108, doi:10.1029/2003JD003405, 2003.

Carslaw, D. C.: The openair manual – open-source tools for analysing air pollution data, Manual for version 0.7-0, King's College, London, 2012.

Carslaw, D. C. and Ropkins, K.: openair – an R package for air quality data analysis, Environ. Modell. Softw., 27–28, 52–61, 2012.

Cavalli, F., Alastuey, A., Areskoug, H., Ceburnis, D., Cech, J., Genberg, J., Harrison, R.M., Jaffrezo, J.L., Kiss, G., Laj, P., Mihalopoulos, N., Perez, N., Quincey, P., Schwarz, J., Sellegri, K., Spindler, G., Swietlicki, E., Theodosi, C., Yttri, K.E., Aas, W., Putaud, J.P.: European aerosol phenomenology -4: Harmonized concentrations of carbonaceous aerosol at 10 regional background sites across Europe, Atmos. Environ.,144, 133-145, 2016.

Chauvigné A., K. Sellegri, M. Hervo, N. Montoux, P. Freville, and Goloub, P.: Comparison of the aerosol optical properties and size disribution retrieved by Sun photometer with in-situ measurements at mid-latitude, Atmos. Meas. Tech., 9, 4569-4585, doi:10.5194/amt-9-4569-2016, 2016.

Colette, A., Aas, W., Banin, L., Braban, C., Ferm, M., González Ortiz, A., Ilyin, I., Mar, K., Pandolfi, M., Putaud, J.-P., Shatalov, V., Solberg, S., Spindler, G., Tarasova, O., Vana, M., Adani, M., Almodovar, P., Berton, E., Bessagnet, B., Bohlin-Nizzetto, P., Boruvkova, J., Breivik, K., Briganti, G., Cappelletti, A., Cuvelier, K., Derwent, R., D'Isidoro, M., Fagerli, H., Funk, C., Garcia Vivanco, M., González Ortiz, A., Haeuber, R., Hueglin, C., Jenkins, S., Kerr, J., de Leeuw, F., Lynch, J., Manders, A., Mircea, M., Pay, M., Pritula, D., Putaud, J.-P., Querol, X., Raffort, V., Reiss, I., Roustan, Y., Sauvage, S., Scavo, K., Simpson, D., Smith, R., Tang, Y., Theobald, M., Tørseth, K., Tsyro, S., van Pul, A., Vidic, S., Wallasch, M., and Wind, P.: Air Pollution trends in the EMEP region between 1990 and 2012., Tech. Rep. Joint Report of the EMEP Task Force on Measurements and Modelling (TFMM), Chemical Co-ordinating Centre (CCC), Meteorological Synthesizing Centre- East (MSC-E), Meteorological Synthesizing Centre-West (MSC-W) EMEP/CCC Report 1/2016, Norwegian Institute for Air Research, Kjeller, Norway, URL http://www.unece.org/fileadmin/DAM/env/documents/2016/AIR/Publications/Air_pollution_trends_in_the_EMEP_region.pdf, 2016., 2016.

Collaud Coen, M., Weingartner, E., Nyeki, S., Cozic, J., Henning, S., Verheggen, B., Gehrig, R., and Baltensperger, U.,: Long-term trend analysis of aerosol variables at the highalpine site Jungfraujoch, J. Geophys. Res., 112, D13213, doi:10.1029/2006JD007995, 2007.

Collaud Coen, M., Weingartner, E., Apituley, A., Ceburnis, D., Fierz-Schmidhauser, R., Flentje, H., Henzing, J. S., Jennings, S. G., Moerman, M., Petzold, A., Schmid, O., and Baltensperger, U.: Minimizing light absorption measurement artifacts of the Aethalometer: evaluation of five correction algorithms, Atmos. Meas. Tech., 3, 457–474, doi:10.5194/amt-3-457-2010, 2010.

Collaud Coen, M., Andrews, E., Asmi, A., Baltensperger, U., Bukowiecki, N., Day, D., Fiebig, M., Fjaeraa, A. M., Flentje, H., Hyvärinen, A., Jefferson, A., Jennings, S. G., Kouvarakis, G., Lihavainen, H., Lund Myhre, C., Malm, W. C., Mihapopoulos, N., Molenar, J. V., O'Dowd, C., Ogren, J. A., Schichtel, B. A., Sheridan, P., Virkkula, A., Weingartner, E., Weller, R., and Laj, P.: Aerosol decadal trends – Part 1: In-situ optical measurements at GAW and IMPROVE stations, Atmos. Chem. Phys., 13, 869-894, doi:10.5194/acp-13-869-2013, 2013.

Collaud Coen, M., Andrews, E., Aliaga, D., Andrade, M., Angelov, H., Bukowiecki, N., Ealo, M., Fialho, P., Flentje, H., Gannet Hallar, A., Hooda, R., Kalapov, I., Krejci, R., Lin, N-H., Marinoni, A., Ming, J., Nguyen, N. A., Pandolfi, M., Pont, V., Ries, L., Rodríguez, S., Schauer, G., Sellegri, K., Sharma, S., Sun, J., Tunved, P., Velasquez, P., and Ruffieux, D.: The topography contribution to the influence of the atmospheric boundary layer at high altitude stations, submitted to Atm. Chem. Phys. Discuss., July 2017.

Crumeyrolle, S., Manninen, H. E., Sellegri, K., Roberts, G., Gomes, L., Kulmala, M., Weigel, R., Laj, P., and Schwarzenboeck, A.: New particle formation events measured on board the ATR-42 aircraft during the EUCAARI campaign, Atmos. Chem. Phys., 10, 6721–6735, doi:10.5194/acp-10-6721-2010, 2010.

Cusack, M., Alastuey, A., Pérez, N., Pey, J., and Querol, X.: Trends of particulate matter (PM2:5) and chemical composition at a regional background site in the Western Mediterranean over the last nine years (2002–2010), Atmos. Chem. Phys., 12, 8341–8357, doi:10.5194/acp-12-8341-2012, 2012.

Delene, D. J. and Ogren, J. A.: Variability of aerosol optical properties at four North American surface monitoring sites, J. Atmos. Sci., 59, 1135–1149, 2002.

Eleftheriadis, K., Ochsenkuhn, K.M., Lymperopoulou, T., Karanasiou, A., Razos, P., Ochsenkuhn-Petropoulou, M.: Influence of local and regional sources on the observed spatial and temporal variability of size resolved atmospheric aerosol mass concentrations and water-soluble species in the Athens metropolitan area, Atm. Environ., 97, 252-261, http://dx.doi.org/10.1016/j.atmosenv.2014.08.013, 2014.

Diaz, A.M., Diaz, J.P., Exposito, F.J., Hernandez-Leal, P.A., Savoie, D., Querol, X.: Air masses and aerosols chemical components in the free troposphere at the subtropical northeast Atlantic region, J. Atmos. Chem., 53, 63–90, 2006.

Diapouli, E., Manousakas, M. I., Vratolis, S., Vasilatou, V., Pateraki, S.,Bairachtari, K. A., Querol, X., Amato, F., Alastuey, A., Karanasiou, A. A., Lucarelli, F., Nava, S., Calzolai, G., Gianelle, V. L., Colombi, C., Alves, C., Custo´dio, D., Pio, C., Spyrou, C., Kallos, G. B., Eleftheriadis, K.: AIRUSE-LIFE +: estimation of natural source contributions to urban ambient air PM10 and PM2:5 concentrations in southern Europe – implications to compliance with limit values. Atmos. Chem. Phys., 17, 3673–3685, 2017..

Doherty, S.J., Quinn, P.K., Jefferson, A., Carrico, C.M., Anderson, T.L., Hegg, D.: A comparison and summary of aerosol optical properties as observed in situ from aircraft, ship, and land during ACE-Asia, J. Geophys. Res., 110, D04201. doi:10.1029/2004JD004964, 2005.

EEA: European Environmental Agency Air quality in Europe – 2013 report, EEA report 9/2013, Copenhagen, 1725–9177, available at: http://www.eea.europa.eu/publications/air-quality-in-europe-2013, 2013.

EEA: European Environmental Agency Air quality in Europe – 2016 report, EEA Report No 28/2016, Copenhagen, available at: file:///D:/Usuari/Descargas/Air%20quality%20in%20Europe%202016%20report%20THAL16027ENN%20(1).pdf, 2016.

EMEP, Transboundary particulate matter in Europe Status report 2008 NILU Reference: O-98134. Edited by Yttri, K.-E., Aas, W., Tørseth, K., Stebel, K., Nyíri, Á., Tsyro, S., Merckova, K., Wankmüller, R., Winiwarter, W., Bauer, H., Caseiro, A., Puxbaum, H., Holzer-Popp, T., Schroedter-Homscheidt, M. (http://tarantula.nilu.no/projects/ccc/reports/emep4-2008.pdf), 2008.

EPA: Emissions of primary particulate matter and secondary particulate matter precursors, Assessment published December 2011, available at: http://www.epa.gov/ttn/chief/trends/, CSI 003, 2011.

Esteve, A.R., Estellés, V., Utrillas, M.P., Martínez-Lozano, J.A.: In-situ integrating nephelometer measurements of the scattering properties of atmospheric aerosols at an urban coastal site in western Mediterranean, Atm. Env., 47, 43-50, 2012.

Fierz-Schmidhauser, R., Zieger, P., Vaishya, A., Monahan, C., Bialek, J., O'Dowd, C. D., Jennings, S. G., Baltensperger, U., Weingartner, E.: Light scattering enhancement factors in the marine boundary layer (Mace Head, Ireland), J. Geophys. Res., 115, D20204, doi:10.1029/2009JD013755, 2010a.

Fierz-Schmidhauser, R., Zieger, P., Gysel, M., Kammermann, L., DeCarlo, P. F., Baltensperger, U., and Weingartner, E.: Measured and predicted aerosol light scattering enhancement factors at the high alpine site Jungfraujoch, Atmos. Chem. Phys., 10, 2319–2333, doi:10.5194/acp-10-2319-2010, 2010b.

Guerreiro, C., Leeuw, F. de, Foltescu, V., Horálek, J., and European Environment Agency: Air quality in Europe 2014 report, Luxembourg: Publications Office, available at: http://bookshop.europa.eu/uri?target=EUB:NOTICE:THAL14005:EN:HTML (last access: 2 June 2016), 2014.

Hansen, J.E. and Travis, L.D.: Light scattering in the planetary atmosphere, Space Science Reviews, 16 527-610, 1974.

Henschel, S., Querol, X., Atkinson, R., Pandolfi, M., Zeca, A., Le Tertre, A., Analitis, A., Katsouyanni, K., Chanel, O., Pascal, M., Bouland, C., Haluza, D., Medina, S., and Goodman, P. G.: Ambient air SO2 patterns in 6 European cities, Atmos. Environ., 79, 236–247, 2013.

Hollander, M., and Wolfe, D. A.: Nonparametric statistical methods, 2nd ed. Wiley, New York, New York, 787, 1999.

IPCC: Climate Change 2014: Synthesis Report. Contribution of Working Groups I, II and III to the Fifth Assessment Report of the Intergovernmental Panel on Climate Change [Core Writing Team, R.K. Pachauri and L.A. Meyer (eds.)]. IPCC, Geneva, Switzerland, 151 pp, 2014.

Kalivitis, N., Bougiatioti, A., Kouvarakis, G., Mihalopoulos, N.: Long term measurements of atmospheric aerosol optical properties in the Eastern Mediterranean, Atmosp. Res., 102, 351–357, 2011.

Karanasiou, A., Querol, X., Alastuey, A., Perez, N., Pey, J., Perrino, C., Berti, G., Gandini, M., Poluzzi, V., Ferrari, S., de la Rosa, J.: Particulate matter and gaseous pollutants in the Mediterranean Basin: Results from the MED-PARTICLES project, Sci. of Tot. Environ., 488–489, 297–315, 2014.

Kecorius, S., Kivekäs, N., Kristensson, A., Tuch, T., Covert, D.S., Birmili, W., Lihavainen, H., Hyvärinen, A.P., Martinsson, J., Sporre, M.K., Swietlicki, E., Wiedensohler, A. Ulevicius, V.: Significant increase of aerosol number concentrations in air masses crossing a densely trafficked sea area, Oceanologia, 58, 1—12, 2016.

Korras-Carraca, M. B., Hatzianastassiou, N., Matsoukas, C., Gkikas, A., and Papadimas, C. D.: The regime of aerosol asymmetry parameter over Europe, the Mediterranean and the Middle East based on MODIS satellite data: evaluation against surface AERONET measurements, Atmos. Chem. Phys., 15, 13113-13132, doi:10.5194/acp-15-13113-2015, 2015.

Laj, P., Klausen, J., Bilde, M., Plaß-Duelmer, C., Pappalardo, G., Clerbaux, C, Baltensperger, U., Hjorth, J., Simpson, D., Reimann, S., Coheur, P.-F., Richter, A., De Mazie, M., Rudich, Y., McFiggans, G., Torseth, K., Wiedensohler, A., Morin, S., Schulz, M., Allan, J. D., Attie, J.-L., Barnes, I., Birmili, W., Cammas, J. P., Dommen, J., Dorn, H.-P., Fowler, D., Fuzzi, S., Glasius, M., Granier, C., Hermann, M., Isaksen, I. S. A., Kinne, S., Koren, I., Madonna, F., Maione, M., Massling, A., Moehler, O., Mona, L., Monks, P. S., Müller , D., Müller , T., Orphal, J., Peuch, V.-H., Stratmann, F., Tanre, D., Tyn dall, F., Abo Riziqmm, A., Van Roozendael, M., Villani P., Wehner, B., Wex, H., and Zardini, A. A.: Measuring atmospheric composition change, Atmos. Environ, 43, 5351–5414, doi:10.1016/j.atmosenv.2009.08.020, 2009.

Li, J., Carlson, B. E., Dubovik, O., and Lacis, A. A.: Recent trends in aerosol optical properties derived from AERONET measurements, Atmos. Chem. Phys., 14, 12271–12289, doi:10.5194/acp-14-12271-2014, 2014.

Lihavainen, H., Hyvärinen, A., Asmi, E., Hatakka, J. and Viisanen, Y.: Long-term variability of aerosol optical properties in northern Finland, Boreal Environment Research, 20, 526–541, 2015a.

Lihavainen, H., Asmi, E., Aaltonen, V., Makkonen, U. and Kerminen, V-M.: Direct radiative feedback due to biogenic secondary organic aerosol estimated from boreal forest site observations, Environ. Res. Lett., 10, doi:10.1088/1748-9326/10/10/104005, 2015b.

Lyamani, H., Olmo, F. J., and Alados-Arboledas, L.: Physical and optical properties of aerosols over an urban location in Spain: seasonal and diurnal variability, Atmos. Chem. Phys., 10, 239-254, doi:10.5194/acp-10-239-2010, 2010.

Lyamani, H., Olmo, F.J., Foyo, I., Alados-Arboledas, L.: Black carbon aerosols over an urban area in south-eastern Spain: Changes detected after the 2008 economic crisis, Atmos. Environ., 45, 6423–6432, 2011.

Lyamani, H., Fernández-Gálvez, J., Pérez-Ramírez, D., Valenzuela, A., Antón, M., Alados, I., Titos, G., Olmo, F.J., Alados-Arboledas, L.: Aerosol properties over two urban sites in South Spain during an extended stagnation episode in winter season, Atmos. Environ., 62, 424-432, 2012.

Ma, N., Birmili, W., Müller, T., Tuch, T., Cheng, Y. F., Xu, W. Y., Zhao, C. S., and Wiedensohler, A.: Tropospheric aerosol scattering and absorption over central Europe: a closure study for the dry particle state, Atmos. Chem. Phys., 14, 6241-6259, doi:10.5194/acp-14-6241-2014, 2014.

Manktelow, P. T., Mann, G. W., Carslaw, K. S., Spracklen, D. V., and Chipperfield, M. P.: Regional and global trends in sulphate aerosol since the 1980's, Geophys. Res. Lett., 34, L14803, doi:10.1029/2006GL028668, 2007.

Marshall, S.F., Covert, D.S., and Charlson, R.J.: Relationship between asymmetry parameter and hemispheric backscatter ratio: implications for climate forcing by aerosols, App. Opt., 34, 27, 6306 – 6311, 1995.

Molnár, A., Bécsi, Z., Imre, K., Gácser, V.,Zita Ferenczi, Z.: Characterization of background aerosol properties during a wintertime smog episode, Aerosol and Air Quality Research, 16, 1793–1804, 2016.

Müller, T., Nowak, A., Weidensohler, A., Sheridan, P., Laborde, M., Covert, D.S., Marinoni, A., Imre, K., Henzing, B., Roger, J.-C., Martins dos Santos, S., Wilhelm, R.,Wang, Y.-Q., de Leeuw, G.: Angular illumination and truncation of three different integrating nephelometers: implications for empirical size-based corrections, Aerosol Sci. Technol., 43, 581–586, 2009.

Müller, T., Laborde, M., Kassell, G., and Wiedensohler, A.: Design and performance of a three-wavelength LED-based total scatter and backscatter integrating nephelometer, Atmos. Meas. Tech., 4, 1291-1303, https://doi.org/10.5194/amt-4-1291-2011, 2011.

Nyeki, S., Baltensperger, U., Colbeck, I., Jost, D.T., Weingartner, E., Gäggeler, H.W.: The Jungfraujoch high-alpine research station (3454 m) as a background continental site for the measurement of aerosol parameters, J. Geophys. Res., 103, 6097-6107, 1998.

Nyeki, S., Halios, C.H., Baum, W., Eleftheriadis, K., Flentje, H., Gröbner, J., Vuilleumier, L., and Wehrli, C.: Ground-based aerosol optical depth trends at three high-altitude sites in Switzerland and southern Germany from 1995 to 2010, J. Geophys. Res., 117, D18202, doi:10.1029/2012JD017493, 2012.

Obiso, V., and Jorba, O.: Impact of aerosol physical properties on atmospheric radiative e ects due to aerosol-radiation interaction, Sci. Tot. Environ., 112, 68-82, 2017.

O'Connor, T.C., Jennings, S.G., O'Dowd, C.D.: Highlights of fifty years of atmospheric aerosol research at Mace Head, Atmos. Res., 90, 338–355, 2008.

Ogren, J. A., Andrews, E., McComiskey, A., Sheridan, P., Jefferson, A., and Fiebig, M.: New insights into aerosol asymmetry parameter, in: Proceedings of the 16th ARM Science Team Meeting, Albuquerque, NM, USA, 2006.

Pandolfi, M., Cusack, M., Alastuey, A., and Querol, X.: Variability of aerosol optical properties in the Western Mediterranean Basin, Atmos. Chem. Phys., 11, 8189–8203, doi:10.5194/acp-11-8189-2011, 2011.

Pandolfi, M., Ripoll, A., Querol, X., and Alastuey, A.: Climatology of aerosol optical properties and black carbon mass absorption cross section at a remote high-altitude site in the western Mediterranean Basin, Atmos. Chem. Phys., 14, 6443-6460, doi:10.5194/acp-14-6443-2014, 2014.

Pandolfi, M., Querol, X., Alastuey, A., Jimenez, J. L., Jorba, O., Day, D., Ortega, A., Cubison, M. J., Comerón, A., Sicard, M., Mohr, C., Prévôt, A. S. H., Minguillón, M. C., Pey, J., Baldasano, J. M., Burkhart, J. F., Seco, R., Peñuelas, J., van Drooge, B. L., Artiñano, B., Di Marco, C., Nemitz, E., Schallhart, S., Metzger, A., Hansel, A., Lorente, J., Ng, S., Jayne, J., and Szidat, S.: Effects of sources and meteorology on particulate matter in the Western Mediterranean Basin: An overview of the DAURE campaign, J. Geophys. Res.-Atmos., 119, 4978–5010, doi:10.1002/2013JD021079, 2014a.

Pandolfi, M., Alastuey, A., Pérez, N., Reche, C., Castro, I., Shatalov, V., and Querol, X.: Trends analysis of PM source contributions and chemical tracers in NE Spain during 2004–2014: a multi-exponential approach, Atmos. Chem. Phys., 16, 11787-11805, doi:10.5194/acp-16-11787-2016, 2016.

Pey, J., Querol, X., Alastuey, A., Forastiere, F., and Stafoggia, M.: African dust outbreaks over the Mediterranean Basin during 2001–2011: PM10 concentrations, phenomenology and trends, and its relation with synoptic and mesoscale meteorology, Atmos. Chem. Phys., 13, 1395–1410, doi:10.5194/acp-13-1395-2013, 2013.

Putaud, J.P., Raes, F., Van Dingenen, R., Brüggemann, E., Facchini, M.C., Decesari, S., Fuzzi, S., Gehrig, R., Hüglin, C., Laj, P., Lorbeer, G., Maenhaut, W., Mihalopoulos, N., Müller, K., Querol, X., Rodriguez, S., Schneider, J., Spindler, G., Ten Brink, H., Tørseth, K., Alfred Wiedensohler, A.: European aerosol phenomenology d2: chemical characteristics of particulate matter at kerbside, urban, rural and background sites in Europe, Atmos. Environ., 38, 2579-2595, 2004.

Putaud, J.P., Van Dingenen, R., Alastuey, A., Bauer, H., Birmili,W., Cyrys, J., Flentje, H., Fuzzi, S., Gehrig, R., Hansson, H.C., Harrison, R.M., Hermann, H., Hitzenberger, R., Hüglin, C., Jones, A.M., Kasper-Giebl, A., Kiss, G., Kousa, A., Kuhlbusch, T.A.J., L€oschau, G., Maenhaut, W., Molnar, A., Moreno, T., Pekkanen, J., Perrino, C., Pitz, M., Puxbaum, H., Querol, X., Rodriguez, S., Salma, I., Schwarz, J., Smolik, J., Schneider, J., Spindler, G., ten Brink, H., Tursic, J., Viana, M., Wiedensohler, A., Raes, F.: A European aerosol

phenomenology d 3: physical and chemical characteristics of particulate matter from 60 rural, urban, and kerbside sites across Europe, Atmos. Environ., 44, 1308-1320, 2010.

Putaud, J. P., Cavalli, F., Martins dos Santos, S., and Dell'Acqua, A.: Long-term trends in aerosol optical characteristics in the Po Valley, Italy, Atmos. Chem. Phys., 14, 9129-9136, doi:10.5194/acp-14-9129-2014, 2014.

Querol, X., Pey, J., Pandolfi, M., Alastuey, A., Cusack, M., Perez, N., Moreno, T., Viana, M., Mihalopoulos, N., Kallos, G., and Kleanthous, S.: African dust contributions to mean ambient PM10 mass-levels across the Mediterranean Basin, Atmos. Environ., 43, 4266–4277, doi:10.1016/j.atmosenv.2009.06.013, 2009.

Querol, X., , Alastuey, A., Pandolfi, M., Reche, C., Pérez, N., Minguillón, M. C., Moreno, T., Viana, M., Escudero, M., Orio, A., Pallarés, M., and Reina, F.: 2001–2012 trends on air quality in Spain, Sci. Total Environ., 490, 957–969, doi:10.1016/j.scitotenv.2014.05.074, 2014.

Revuelta, M.A., Artiñano, B., Gómez-Moreno, F.J., Viana, M., Reche, C., Querol, X., Fernández, A.J., Mosquera, J.L., Núñez, L., Pujadas, M., Herranz, A., López, B., Molero, F., Bezares, J.C., Coz, E., Palacios, M., Sastre, M., Férnandez, J.M., Salvador, P., Aceña, B.: Ammonia levels in different kinds of sampling sites in the central Iberian Peninsula, Proceedings of the 2nd Iberian meeting on aerosol science and technology, RICTA 2014.

Rodríguez, S., Alastuey, A., Alonso-Pérez, S., Querol, X., Cuevas, E., Abreu-Afonso, J., Viana, M., Pérez, N., Pandolfi, M., and de la Rosa, J.: Transport of desert dust mixed with North African industrial pollutants in the subtropical Saharan Air Layer, Atmos. Chem. Phys., 11, 6663-6685, doi:10.5194/acp-11-6663-2011, 2011.

Rose C., K. Sellegri, Fernando Velarde, Isabel Moreno, Kay Weinhold, Ali Wiedensholer, and Laj, P.: Frequent nucleation events at the high altitude station of Chacaltaya (5240 m a.s.l.), Bolivia, Atmos. Environ., 102, 18-29, doi :10.1016/j.atmosenv.2014.11.015, 2015.

Rotstayn, L. D., Collier, M. A., Chrastansky, A., Jeffrey, S. J., and Luo, J.-J.: Projected effects of declining aerosols in RCP4.5: unmasking global warming?, Atmos. Chem. Phys., 13, 10883-10905, doi:10.5194/acp-13-10883-2013, 2013.

Schuster, G. L., Dubovik, O., and Holben, B. N.: Angstrom exponent and bimodal aerosol size distributions, J. Geophys. Res., 111, D07207, doi:101029/2005JD006328, 2006.

Seinfeld, J. H. and Pandis, S. N.: Atmospheric Chemistry and Physics, John Wiley and Sons, New York, 1998.

Sen, P. K.: Estimates of regression coefficient based on Kendall's tau, J. Am. Stat. Assoc., 63, 1379–1389, 1968.

Spindler, G., Bruggemann, E., Gnauk, T., Gruner, Müller , A. K., Herrmann, H.: A four-year size-segregated characterization study of particles PM10, PM2.5 and PM1 depending on air mass origin at Melpitz, Atmos. Environ.,44, 164-173, 2010.

Stohl, A., Aamaas, B., Amann, M., Baker, L. H., Bellouin, N., Berntsen, T. K., Boucher, O., Cherian, R., Collins, W., Daskalakis, N., Dusinska, M., Eckhardt, S., Fuglestvedt, J. S., Harju, M., Heyes, C., Hodnebrog, Ø., Hao, J., Im, U., Kanakidou, M., Klimont, Z., Kupiainen, K., Law, K. S., Lund, M. T., Maas, R., MacIntosh, C. R., Myhre, G., Myriokefalitakis, S., Olivié, D., Quaas, J., Quennehen, B., Raut, J.-C., Rumbold, S. T., Samset, B. H., Schulz, M., Seland, Ø., Shine, K. P., Skeie, R. B., Wang, S., Yttri, K. E., and Zhu, T.: Evaluating the climate and air quality impacts of short-lived pollutants, Atmos. Chem. Phys., 15, 10529-10566, doi:10.5194/acp-15-10529-2015, 2015.

Theil, H.: A rank invariant method of linear and polynomial regression analysis, I, II, III, Proceedings of the Koninklijke Nederlandse Akademie Wetenschappen, Series A, Mathematical Sciences, 386–392, 521–525, 1397–1412, 1950.

Titos, G., Foyo-Moreno, I., Lyamani, H., Querol, X., Alastuey, A., Alados-Arboledas, L.: Optical properties and chemical composition of aerosol particles at an urban location: An estimation of the aerosol mass scattering and absorption efficiencies, J. Geophys. Res. Atm., 117, 4, D04206, 2012.

Titos, G., Lyamani, H., Pandolfi, M., Alastuey, A., Alados-Arboledas, L.: Identification of fine (PM1) and coarse (PM10-1) sources of particulate matter in an urban environment, Atmos. Environ., 89, 593-602, 2014.

Titos, G., del Águila, A., Cazorla, A., Lyamani, H., Casquero-Vera, J.A., Colombi, C., Cuccia, E., Gianelle, V., Močnik, G., Alastuey, A., Olmo, F.J., Alados-Arboledas, L.: Spatial and temporal variability of carbonaceous aerosols: Assessing the impact of biomass burning in the urban environment, Sci. of Tot. Environ., 578, 613-625, 2017.

Tørseth, K., Aas, W., Breivik, K., Fjæraa, A. M., Fiebig, M., Hjellbrekke, A. G., Lund Myhre, C., Solberg, S., and Yttri, K. E.: Introduction to the European Monitoring and Evaluation Programme (EMEP) and observed atmospheric composition change during 1972–2009, Atmos. Chem. Phys., 12, 5447–5481, doi:10.5194/acp-12-5447-2012, 2012.

Tunved,P., Hansson, H.-C., Kerminen, V.-M., Ström, J., Dal Maso, M., Lihavainen, H., Viisanen, Y., Aalto, P. P., Komppula, M., Kulmala, M.: High Natural Aerosol Loading over Boreal Forests, Science, 312, 5771, 261-263, DOI: 10.1126/science.1123052, 2006.

Valenzuela, A., Olmo, F.J., Lyamani, H., Antón, M., Titos, G., Cazorla, A., Alados-Arboledas, L.: Aerosol scattering and absorption Angström exponents as indicators of dust and dust-free days over Granada (Spain), Atmos. Res., 154, 1-13, 2015.

Van Dingenen, R., Putaud, J.P., Raes, F., Baltensperger, U., Charron, A., Facchini, M.C., Decesari, S., Fuzzi, S., Gehrig, R., Hansson, H.C., Harrison, R.M., Hüglin, C., Jones, A.M., Laj, P., Lorbeer, G., Maenhaut, W., Palgren, F., Querol, X., Rodriguez, S., Schneider, J., Ten Brink, H., Tunved, P., Tørseth, K., Wehner, B., Weingartner, E., Wiedensohler, A., Wåhlin, P.: A European aerosol phenomenology_1: physical characteristics of particulate matter at kerbside, urban, rural and background sites in Europe, Atmos. Environ., 38, 2561-2577, 2004.

van Donkelaar, A., Randall, M., Brauer, M., Kahn, R., Levy, R., Verduzco, C., and Villeneuve, P. J. Global estimates of exposure to fine particulate matter concentrations from satellite-based aerosol optical depth, Environ. Health Persp., 118, 847–855, doi:10.1289/ehp.0901623, 2010.

Venzac, H., Sellegri, K., Villani, P., Picard, D., and Laj, P.: Seasonal variation of aerosol size distributions in the free troposphere and residual layer at the puy de Dome station, France, Atmos. Chem. Phys., 9, 1465–1478, doi:10.5194/acp-9-1465-2009, 2009.

Virkkula, A., Backman, J., Aalto, P. P., Hulkkonen, M., Riuttanen, L., Nieminen, T., dal Maso, M., Sogacheva, L., de Leeuw, G., and Kulmala, M.: Seasonal cycle, size dependencies, and source analyses of aerosol optical properties at the SMEAR II measurement station in Hyytiälä, Finland, Atmos. Chem. Phys., 11, 4445–4468, doi:10.5194/acp-11-4445-2011, 2011.

Vrekoussis, M., Liakakou, E., Koc-ak, M., Kubilay, N., Oikonomou,1, K., Sciare, J., Mihalopoulos, N.: Seasonal variability of optical properties of aerosols in the Eastern Mediterranean, Atmosp. Environ., 39, 7083–7094, 2005.

WMO/GAW report 227: Aerosol Measurement Procedures, Guidelines and Recommendations, 2nd Edition, 2016, 103 pp. August 2016 (WMO-No. 1177).

Zanatta, M., Gysel, M., Bukowiecki, N., Müller, T., Weingartner, E., Areskoug, H., Fiebig, M., Yttri, K.E., Mihalopoulos, N., Kouvarakis, G., Beddows, D., Harrison, R.M., Cavalli, F., Putaud, J.P., Spindler, G., Wiedensohler, A., Alastuey, A., Pandolfi, M., Sellegri, K., Swietlicki, E., Jaffrezo, J.L., Baltensperger, U., Laj, P.: A European aerosol phenomenology-5: Climatology of black carbon optical properties at 9 regional background sites across Europe, Atm. Env., 145, 346-364, 2016.

Zieger, P., Kienast-Sjögren, E., Starace, M., von Bismarck, J., Bukowiecki, N., Baltensperger, U., Wienhold, F. G., Peter, T., Ruhtz, T., Collaud Coen, M., Vuilleumier, L., Maier, O., Emili, E., Popp, C., and Weingartner, E.: Spatial variation of aerosol optical properties around the high-alpine site Jungfraujoch (3580 m a.s.l.), Atmos. Chem. Phys., 12, 7231-7249, doi:10.5194/acp-12-7231-2012, 2012.

Atmos. Chem. Phys. Discuss., https://doi.org/10.5194/acp-2017-826
Manuscript under review for journal Atmos. Chem. Phys.
Discussion started: 13 October 2017

Atmospheric Chemistry and Physics Discussions

1 **Tables**
2
3 **Table 1:** List of ACTRIS observatories providing aerosol particle scattering measurements

Observatory name	*Country*	*Observatory code*	*Lat, Long*	*Altitude [m a.s.l.]*	*Placement (from EBAS metadata)*	*Inlet*	*Nephelometer model*	*Period (a)*
nordic and Baltic								
Birkenes II **(BIR)**	Norway	NO0002R	58.3885 N, 8.252 E	219	regional	PM_{10}	TSI3563	07/2009 –12/2015
Hyytiälä **(SMR)**	Finland	FI0050R	61.85N, 24.2833 E	181	regional	PM_{10}	TSI3563	05/2006 –12/2015
Pallas **(PAL)**	Finland	FI0096G	67.97 N, 24.12 E	565	continental	PM_5; $PM_{2.5}$; PM_{10} (*b*)	TSI3563	02/2000 –12/2015
Vavihill **(VHL)**	Sweden	SE0011R	56.0167 N, 13.15 E	175	continental	PM_{10}	ECOTECH Aurora3000	03/2008 –04/2014
Preila **(PLA)**	Lithuania	LT0015R	55.35 N, 21.0667 E	5	coastal/marine	PM_{10}	TSI3563	12/2012 –04/2014
western								
Mace Head **(MHD)**	Ireland	IE0031R	53.3258 N, -9.8994 E	5	coastal/marine	whole air	TSI3563	07/2001 –12/2013
Cabauw **(CBW)**	The Netherlands	NL0011R	51.9703 N, 4.9264 E	1	regional	PM_{10}	TSI3563	01/2008 –12/2012
SIRTA **(SIR)**	France	FR0020R	48.7086 N, 2.1589 E	162	suburban	whole air	ECOTECH M9003	07/2012 –12/2013
Observatory Perenne **(OPE)**	France	FR0022R	48.5622 N, 5.505555 E	392	regional	whole air; PM_{10} (*c*)	ECOTECH Aurora3000	09/2012 –12/2015
Puy de Dome **(PUY)**	France	FR0030R	45.7667 N, 2.95 E	1465	mountain	whole air	TSI3563	01/2007 –12/2014
central								
Hohenpeissenberg **(HPB)**	Germany	DE0043G	47.8 N, 11.0167 E	985	mountain	PM_{10}	TSI3563	01/2006 –12/2015
Ispra **(IPR)**	Italy	IT0004R	45.8 N, 8.6333 E	209	semi regional	PM_{10}	TSI3563	01/2004 –12/2014
Melpitz **(MPZ)**	Germany	DE0044R	51.53 N, 12.93 E	86	regional	PM_{10}	TSI3563	01/2007 –12/2015
Jungfraujoch **(JFJ)**	Switzerland	CH0001G	46.5475 N, 7.985 E	3578	mountain	whole air	TSI3563	07/1995 –12/2015
Mt. Cimone **(CMN)**	Italy	IT0009R	44.1833 N, 10.7 E	2165	mountain	whole air	ECOTECH Aurora M9003; TSI 3563 (*d*)	05/2007 –12/2015
Košetice **(KOS)**	Czech Republic	CZ0007R	49.58333N, 15.0833 E	534	regional	PM_{10}	TSI3563	03/2013 – 12/2015
eastern								
Beo Moussala **(BEO)**	Bulgaria	BG0001R	42.1667 N, 23.5833 E	2971	mountain	whole air	TSI3563	03/2007 –12/2015
K-Puszta **(KPS)**	Hungary	HU0002R	46.9667 N, 19.5833 E	125	regional	PM_1; PM_{10} (*e*)	TSI3563	05/2006 –12/2014
south-western								
Montsec **(MSA)**	Spain	ES0022R	42.0513 N, 0.44 E	1570	mountain	$PM_{2.5}$; PM_{10} (*f*)	ECOTECH Aurora3000	01/2013 – 12/2015
Izaña **(IZO)**	Spain	ES0018G	28.309 N, -16.4994 E	2373	mountain	PM_{10}	TSI3563	03/2008 – 12/2015
Granada **(UGR)**	Spain	ES0020U	37.164 N, -3.605 E	680	urban	whole air	TSI3563	01/2006 –12/2015
Montseny **(MSY)**	Spain	ES1778R	41.7667 N, 2.35 E	700	regional	PM_{10}	ECOTECH Aurora3000	01/2010 –12/2015
Madrid **(MAD)**	Spain	ES1778R	40.4627 N, -3.717 E	669	sub-urban	$PM_{2.5}$; PM_{10} (*g*)	ECOTECH Aurora3000	01/2014 – 12/2014
south-eastern								
Finokalia **(FKL)**	Greece	GR0002R	35.3167 N, 25.6667 E	250	coastal/marine	whole air; PM_1; PM_{10} (*h*)	RR M903; Ecotech Aurora1000 (i)	04/2004 –12/2015
Athens **(DEM)**	Greece	GR0100B	37.9905 N, 23.8095 E	270	sub-urban	PM_{10}	ECOTECH Aurora3000	01/2012 –12/2015
Arctic								

Zeppelin **(ZEP)**	Svalbard (Norway)	NO0042G	78.9067 N, 11.8883 E	474	arctic environment	PM_{10}	TSI3563	07/2010 –12/2014
Antarctic								
Troll **(TRL)**	Antarctica	NO0058G	-72.0167 N, 2.5333 E	1309	antarctic environment	whole air; PM_{10} *(j)*	TSI3563	02/2007 –12/2015
South America								
Mt. Chacaltaya **(CHC)**	Bolivia	BO0001R	-16.2000 N, -68.09999 E	5240	mountain	whole air	ECOTECH Aurora3000	01/2012 – 12/2015 (*k*)

(a) Start-end of measurements; Total aerosol particle scattering was used as reference for measurement period; (b) PM_5 (2000-2005), $PM_{2.5}$ (2005-2008) and PM_{10} (2008-2015); (c) whole air (2012-2013) and PM_{10} (2014-2015); (d) ECOTECH Aurora M9003 during 2007-2013 and TSI 3563 (2014-2015); (e) PM_1 (2006-04/2008) and PM_{10} (05/2008-2014); (f) $PM_{2.5}$ (2013) and PM_{10} (2014-2015); (g) PM_{10} from 03/2014; (h) whole air (2004-2008), PM_{10} (2009-2011), PM_1 (2011-2012), PM_{10} (2013-2015); (i) RR M903 during 2004-2011, Ecotech AURORA1000 during 2012-2015; (j) whole air (2007-2009) and PM_{10} (2010-2015); (k) Only measurements performed during the year 2012 were used in this investigation.

Atmos. Chem. Phys. Discuss., https://doi.org/10.5194/acp-2017-826
Manuscript under review for journal Atmos. Chem. Phys.
Discussion started: 13 October 2017

Atmospheric Chemistry and Physics Discussions

Table 2: Trends of aerosol particle scattering coefficient (σ_{sp}), scattering Ångström exponent (SAE), and backscatter fraction (BF). Three trends for SAE are reported: SAE calculated as linear fit using three wavelengths (b-g-r); using the blue and the green wavelengths (b-g) and using the green and red wavelengths (g-r). Trend results are reported for the whole period available at each station until 2015 (bold) and for the periods reported in Collaud Coen et al. (2013) and in Asmi et al. (2013). Trends are considered as statistically significant if p-value < 0.05. Statistically significant increasing or decreasing trends are highlighted with up (↑) and down (↓) red and green arrows, respectively. Non-statistically significant increasing or decreasing trends are highlighted with up (↑) and down (↓) grey arrows, respectively. Grey colored table cells highlight stations included in this work but not included in the works from Collaud Coen et al. (2013) or Asmi et al. (2013). $: parameters removed in this work and in the work from Collaud Coen et al. (2013) because of measurement gaps, low data coverage or break points for one or more wavelengths. #: Only available for 2014-2015; ± not available.

		Trend (This work)					MK Trend (Collaud Coen et al., 2013)					MK Trend (Asmi et al., 2013)		
			SAE					SAE				Particle number		
Station	period	σ_{sp}	b-g-r	b-g	g-r	BF	σ_{sp}	b-r	b-g	g-r	BF	N	N20 (20-500 nm)	N100 (100-500 nm)
Nordic and Baltic														
PAL	**2000 - 2015**	↑	↓	↓	↓	↑								
	2000 - 2010	↓	↓	$	$	↑	↓	↑	$	$	↑			
	2001 - 2010	↓	↓	$	$	↑	↓	↑	$	$	↑	↓ (10-500 nm)	↔	↑
	1996 - 2010											↓ (10-500 nm)		
SMR	**2006 - 2015**	↓	↑	↑	↑	↑								
	1996 - 2011												↓	↓
	2001 - 2010												↓	↓
western														
MHD	**2001 - 2013**	↓	$	$	$	$								
	2000 - 2010											↓ (3-500 nm)		
	2001 - 2010	↑	$	$	$	$	↑	$	$	$	$	↑ (3-500 nm)		
PUY	**2007 - 2014**	↓	↓	↓	↓	↑								
central														
HPB	**2006 - 2015**	↓	↑	↑	↑	↑								
	2001 - 2010						↑	$	$	$	$			
	2002 - 2010						↓	$	$	$	$			
	1995 - 2011											↑ (15-500 nm)		
IPR	**2004 - 2014**	↓	↑	↑	↑	↑								
MPZ	**2007 - 2015**	↓	↓	↓	↓	↑								
	1997 – 1998 and 2004 - 2010												↑	↑
JFJ	**1995 - 2015**	↓	$	$	$	$								
	1995 - 2010	↑	$	$	$	$	↑	$	$	$	$			
	1996 - 2010	↑	$	$	$	$	↑	$	$	$	$			
	2001 - 2010	↓	$	$	$	$	↓	$	$	$	$	↓ (10-500 nm)		
	1997 - 2010	↑	$	$	$	$						↑ (10-500 nm)		
CMN	**2007 - 2015**	↓	#	#	#	#								
eastern														
BEO	**2007 - 2015**	↓	↓	↓	↓	↓								

KPS	2006 - 2014	↑	↓	↓	↑	↑								
south-western														
IZO	2008 - 2015	↓	↑	↑	↑	$								
UGR	2006 - 2015	↓	↑	↑	↑	↑								

Table 3: Daytime (08:00 – 16:00 GMT) and nighttime (21:00 – 05:00 GMT) of σ_{sp} trends by season calculated for the periods considered in this work. Sp: Spring; Su: Summer; Au: Autumn; Wi: Winter. Trends are considered as statistically significant if p-value < 0.05. Statistically significant increasing or decreasing trends are highlighted with up (↑) and down (↓) red and green arrows, respectively. Non statistically significant increasing or decreasing trends are highlighted with up (↑) and down (↓) grey arrows, respectively.

Station	***period***	***SCATTERING***					
		daytime		*nighttime*		*24h*	
		Sp	*Su*	*Sp*	*Su*	*Sp*	*Su*
		Au	*Wi*	*Au*	*Wi*	*Au*	*Wi*
JFJ	1995 - 2015	↓	↓	↓	↓	↓	↓
		↑	↓	↑	↓	↑	↓
HPB	2006 - 2015	↓	↓	↓	↓	↓	↓
		↓	↓	↓	↓	↓	↓
PUY	2006 - 2014	↓	↓	↓	↓	↓	↓
		↓	↓	↓	↓	↓	↓
CMN	2007 - 2015	↓	↑	↓	↓	↓	↓
		↓	↓	↓	↓	↓	↓
BEO	2007 - 2015	↓	↓	↓	↑	↓	↓
		↓	↓	↓	↑	↓	↑
IZO	2008 - 2015	↓	↓	↓	↓	↓	↓
		↑	↓	↑	↓	↑	↓

Atmos. Chem. Phys. Discuss., https://doi.org/10.5194/acp-2017-826
Manuscript under review for journal Atmos. Chem. Phys.
Discussion started: 13 October 2017

Atmospheric Chemistry and Physics Discussions

Figures

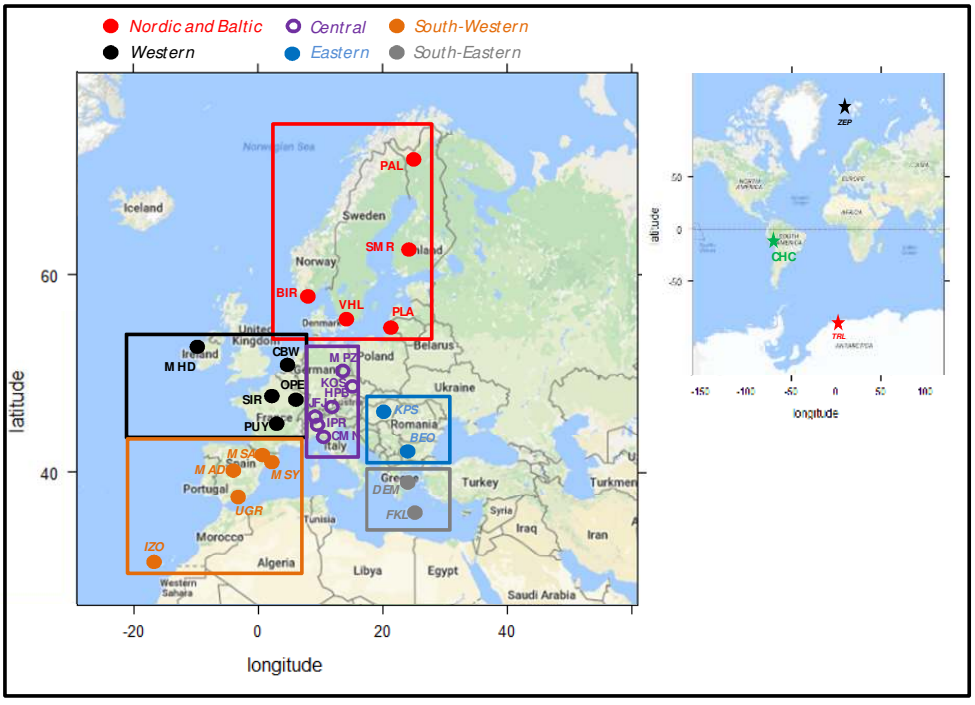

Figure 1: Location of the 28 ACTRIS stations included in this work.

Atmos. Chem. Phys. Discuss., https://doi.org/10.5194/acp-2017-826
Manuscript under review for journal Atmos. Chem. Phys.
Discussion started: 13 October 2017

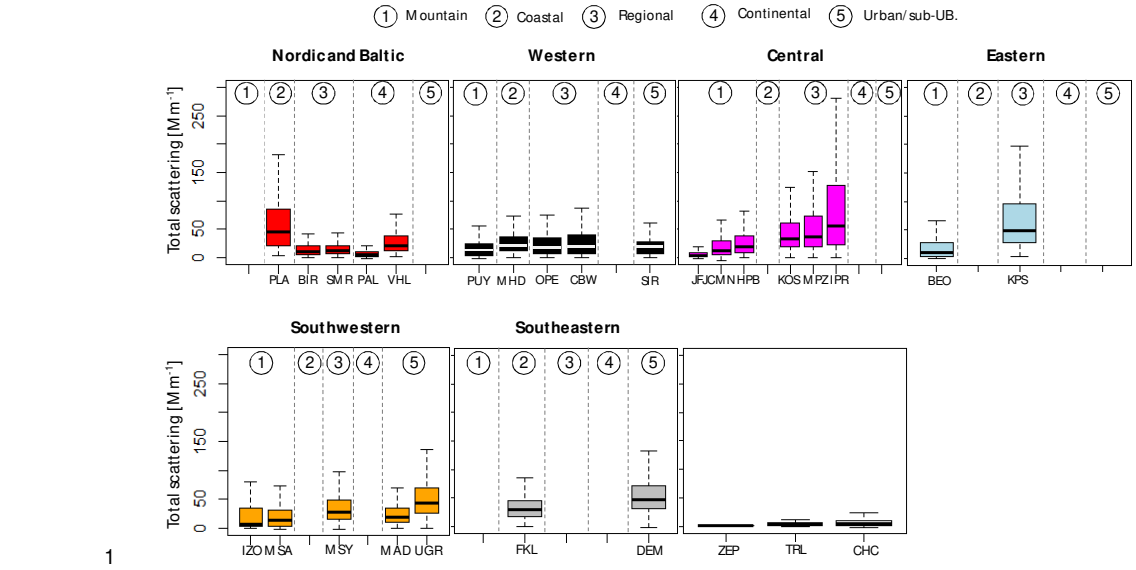

Figure 2: Total aerosol scattering coefficients in the green divided by geographical location. At SIR aerosol scattering was available only at 450 nm. Medians (horizontal lines in the boxes), percentiles 25th and 75th (lower and upper limits of the boxes, respectively) and percentiles 5th and 95th (lower and upper limits of the vertical dashed lines) are reported. Hourly data were used for the statistic. For each location data are ordered from mountain sites (1) to urban/sub-urban sites (5).

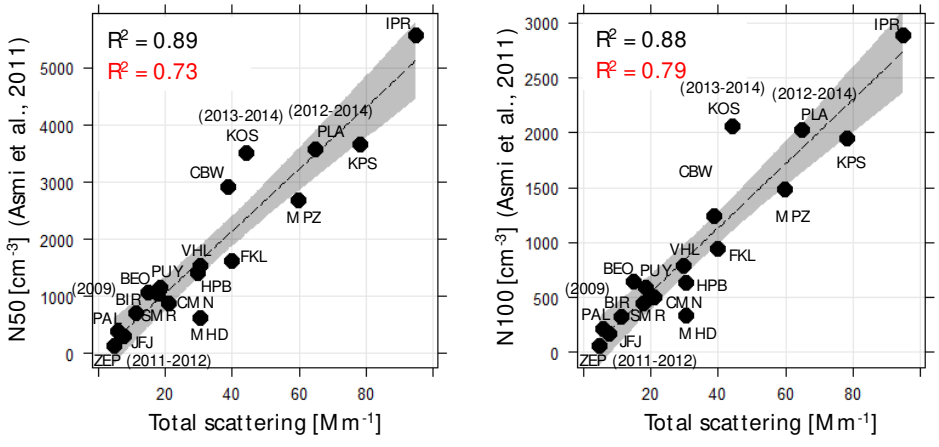

Figure 3: Relationship between N50 (mean particle number concentration between 50 nm and 500 nm) and N100 (mean particle number concentration between 100 nm and 500 nm) and mean aerosol particle scattering coefficient averaged over the period 2008 – 2009. For ZEP, BIR, KOS and PLA aerosol particle scattering measurements were not available during 2008 – 2009 and different period were used. R^2 highlighted in red were obtained using the median values.

Atmos. Chem. Phys. Discuss., https://doi.org/10.5194/acp-2017-826
Manuscript under review for journal Atmos. Chem. Phys.
Discussion started: 13 October 2017

Atmospheric Chemistry and Physics Discussions

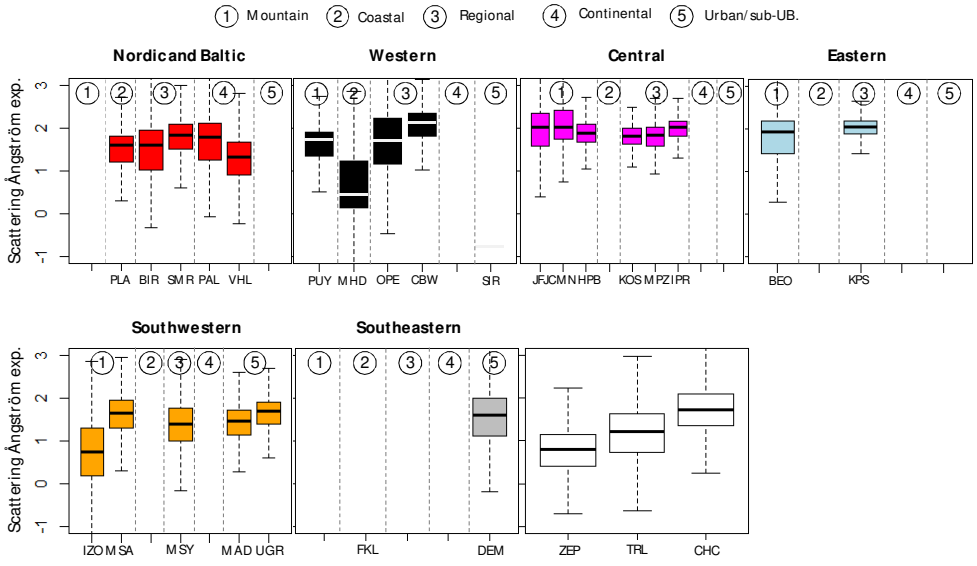

Figure 4: Scattering Ångström exponent divided by geographical location. Medians (horizontal lines in the boxes), percentiles 25th and 75th (lower and upper limits of the boxes, respectively) and percentiles 5th and 95th (lower and upper limits of the vertical dashed lines) are reported. For each location data are ordered from mountain sites to urban/sub-urban sites. At CHC, the SAE was calculated using the blue and green wavelengths.

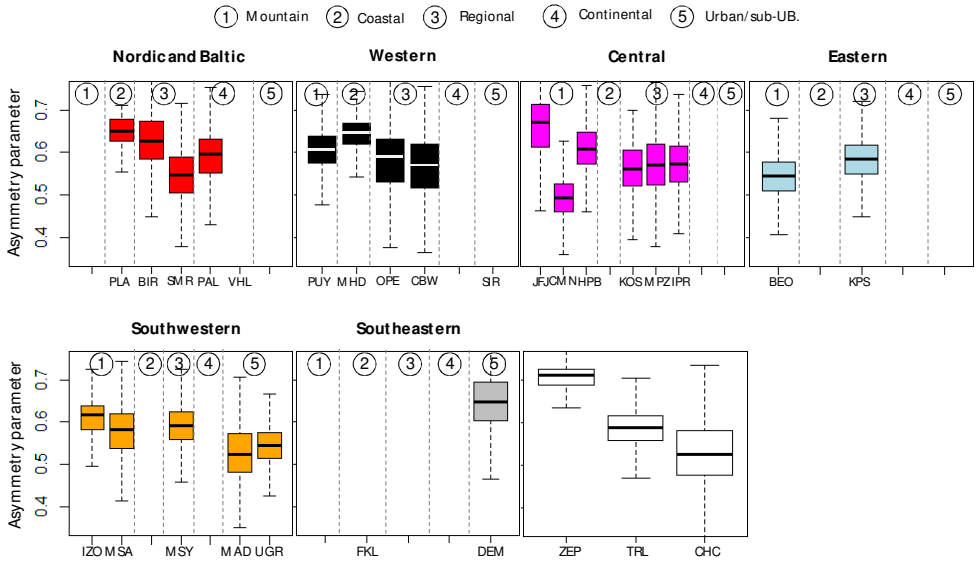

Figure 5: Asymmetry parameter in the green divided by geographical location. Medians (horizontal lines in the boxes), percentiles 25th and 75th (lower and upper limits of the boxes, respectively) and percentiles 5th and 95th (lower and upper limits of the vertical dashed lines) are reported. For each location data are ordered from mountain sites to urban/sub-urban sites.

Atmos. Chem. Phys. Discuss., https://doi.org/10.5194/acp-2017-826
Manuscript under review for journal Atmos. Chem. Phys.
Discussion started: 13 October 2017

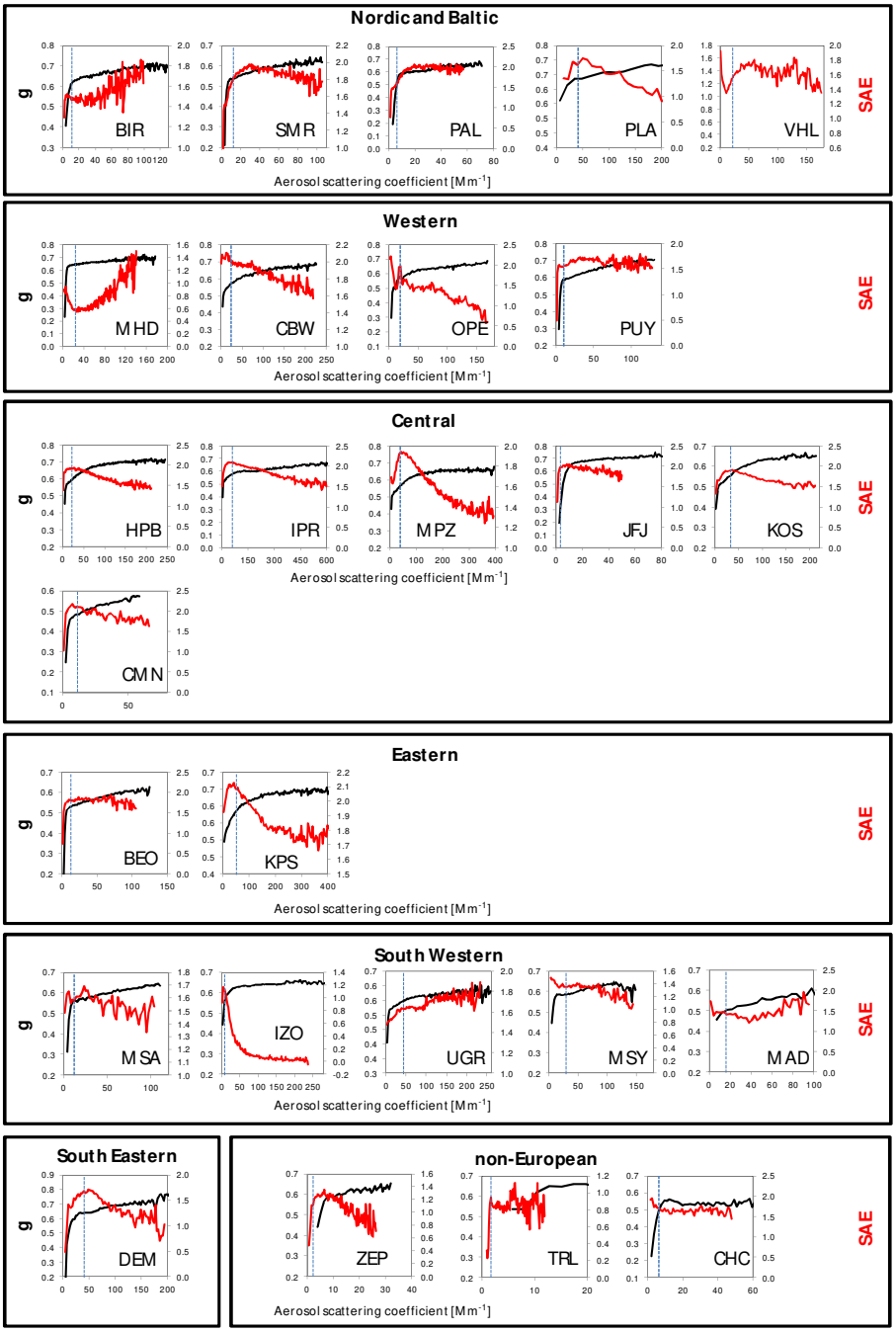

Figure 6: Scatterplots between σ_{sp} (x-axes) and SAE (right y-axes; red lines) and *g* (left y-axes; black lines). Dashed lines represent median σ_{sp} values at each station. At CHC, SAE was calculated using the blue and the green wavelengths.

Atmos. Chem. Phys. Discuss., https://doi.org/10.5194/acp-2017-826
Manuscript under review for journal Atmos. Chem. Phys.
Discussion started: 13 October 2017

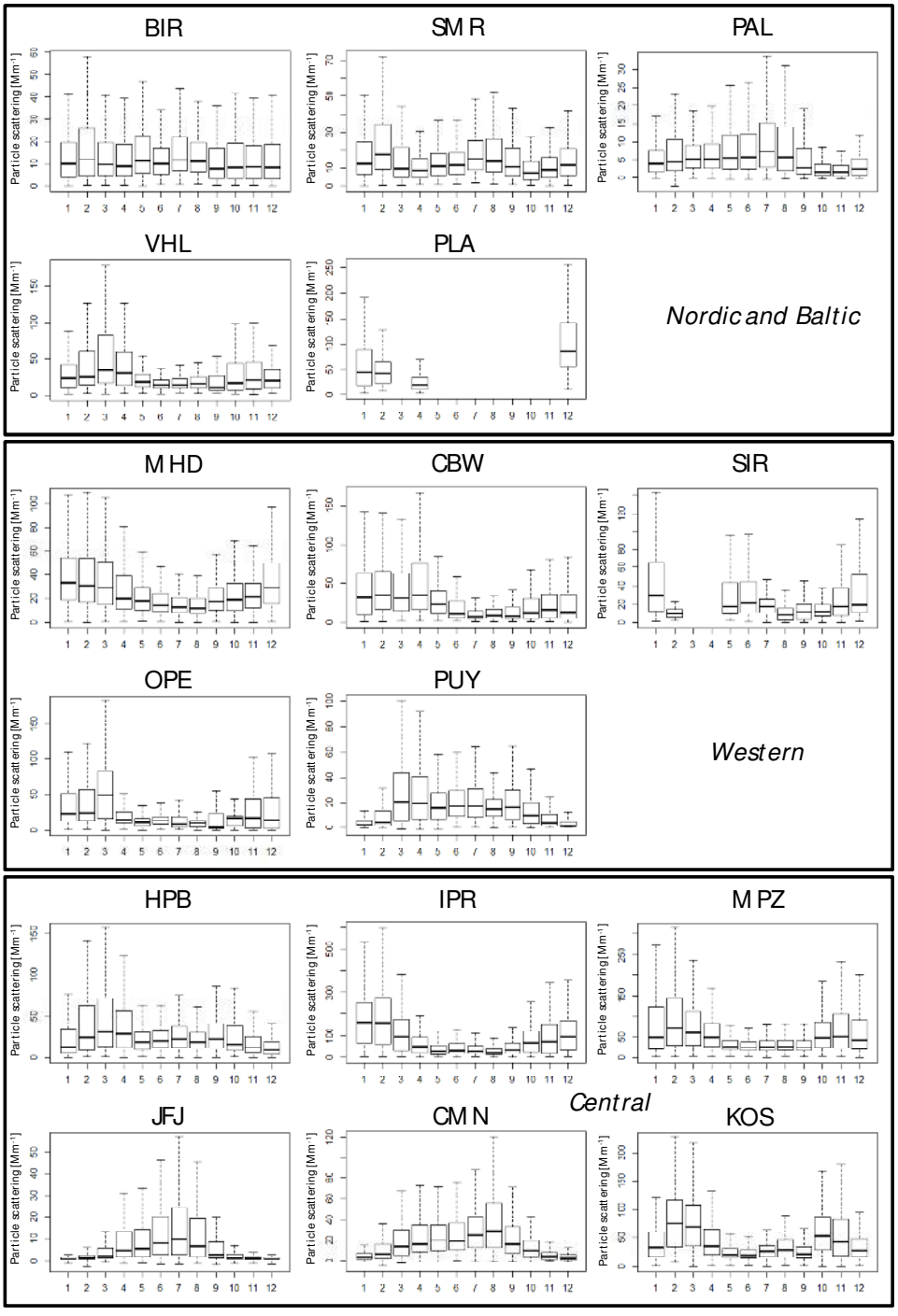

Figure 7: Seasonal cycles of σ_{sp} [Mm^{-1}] measured in the green nephelometer wavelength.

Atmos. Chem. Phys. Discuss., https://doi.org/10.5194/acp-2017-826
Manuscript under review for journal Atmos. Chem. Phys.
Discussion started: 13 October 2017

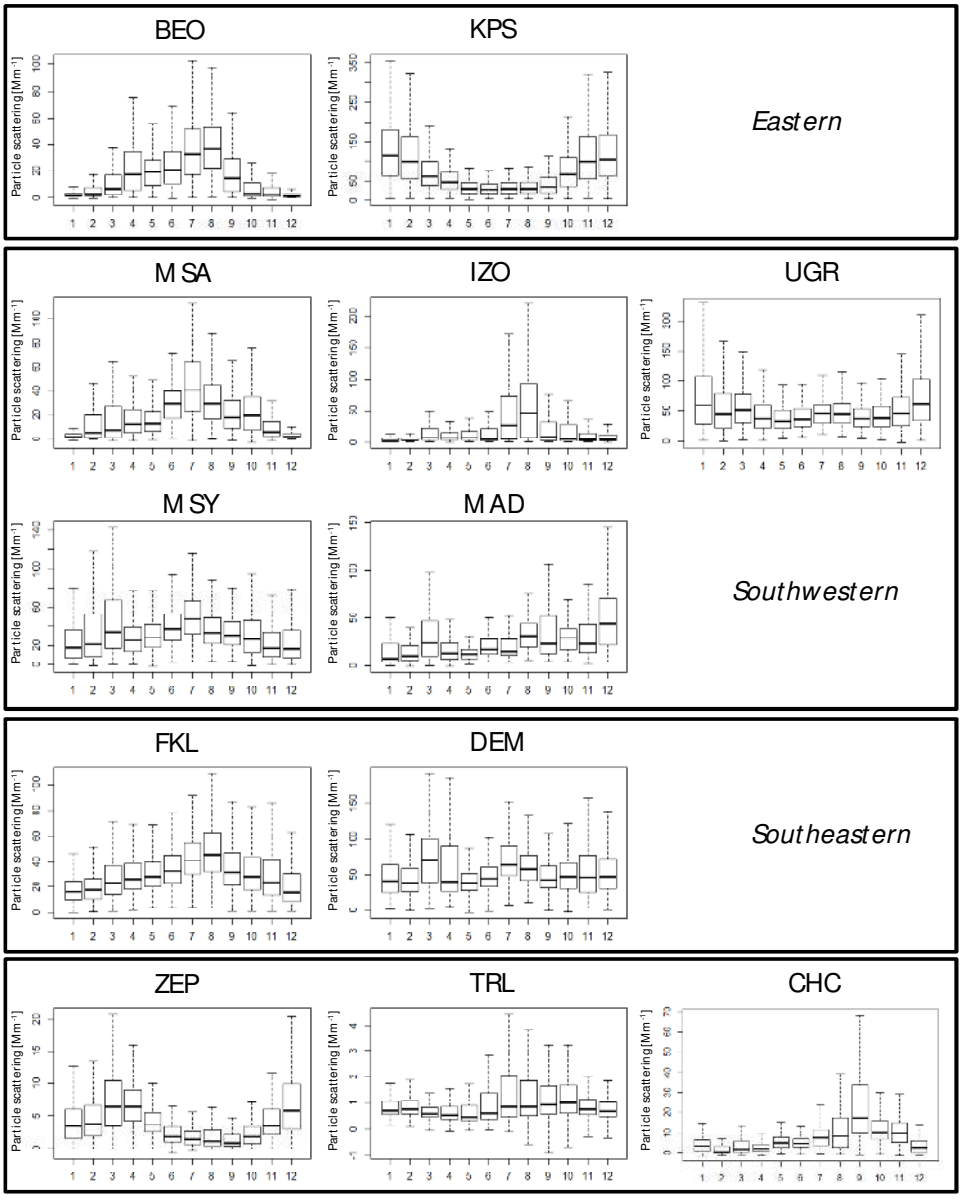

Figure 7: (Continued) Seasonal cycles of σ_{sp} [Mm^{-1}] measured in the green nephelometer wavelength.

Atmos. Chem. Phys. Discuss., https://doi.org/10.5194/acp-2017-826
Manuscript under review for journal Atmos. Chem. Phys.
Discussion started: 13 October 2017

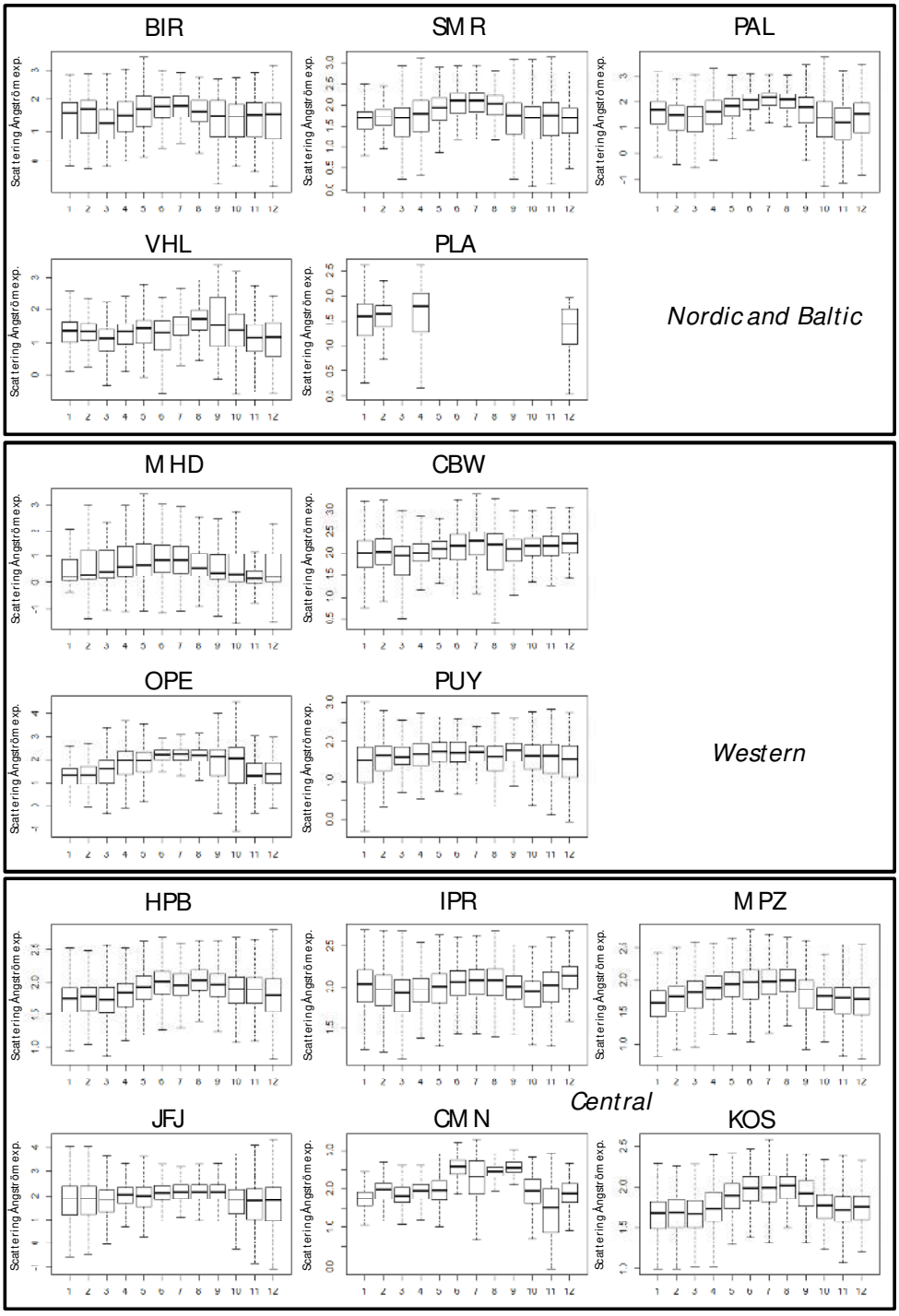

Figure 8: Seasonal cycles of SAE (calculated as linear fit using three nephelometer wavelengths)

Atmos. Chem. Phys. Discuss., https://doi.org/10.5194/acp-2017-826
Manuscript under review for journal Atmos. Chem. Phys.
Discussion started: 13 October 2017

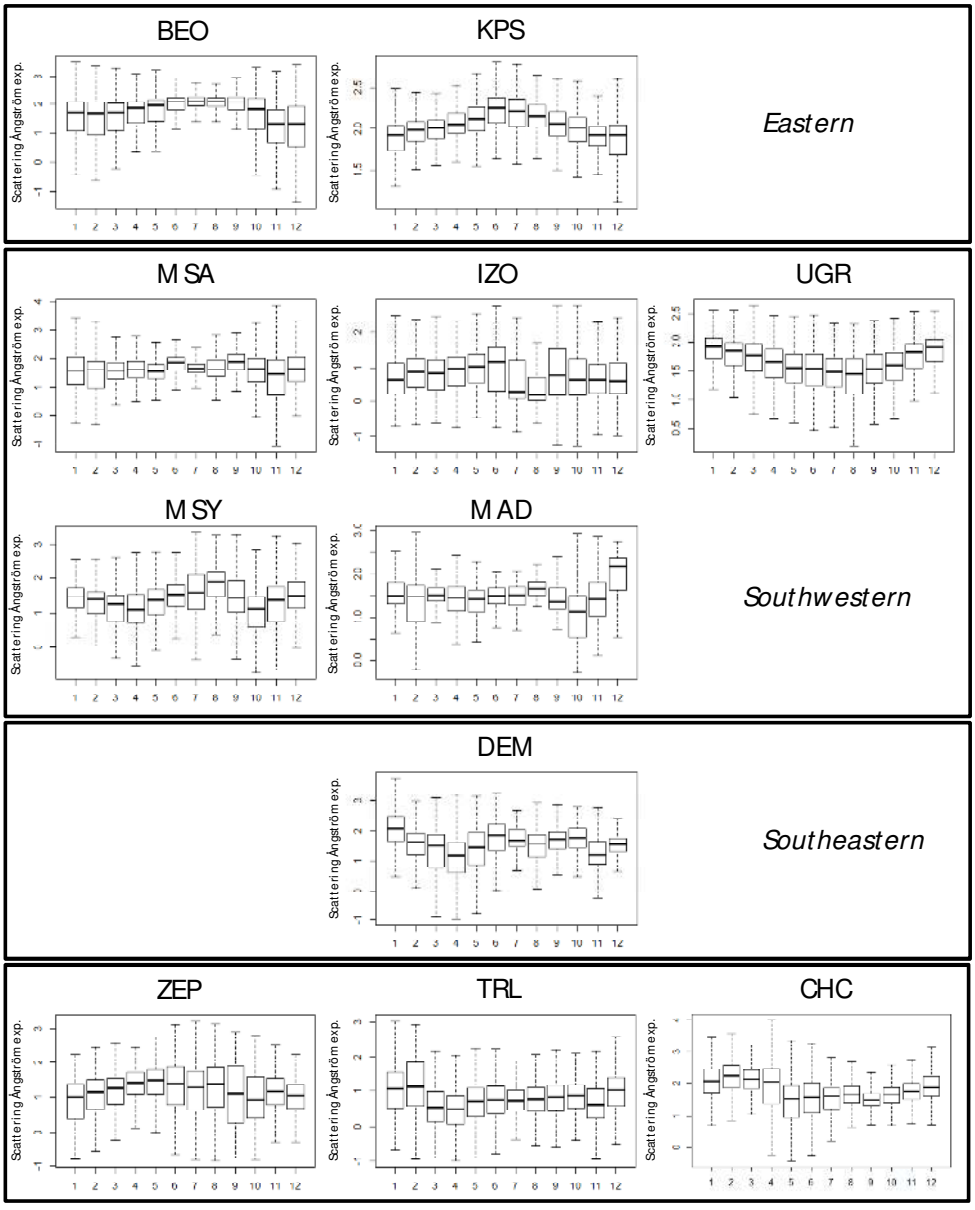

Figure 8: (Continued) Seasonal cycles of SAE (calculated as linear fit using three nephelometer wavelengths). At CHC the SAE was calculated using the blue and the green wavelengths.

Atmos. Chem. Phys. Discuss., https://doi.org/10.5194/acp-2017-826
Manuscript under review for journal Atmos. Chem. Phys.
Discussion started: 13 October 2017

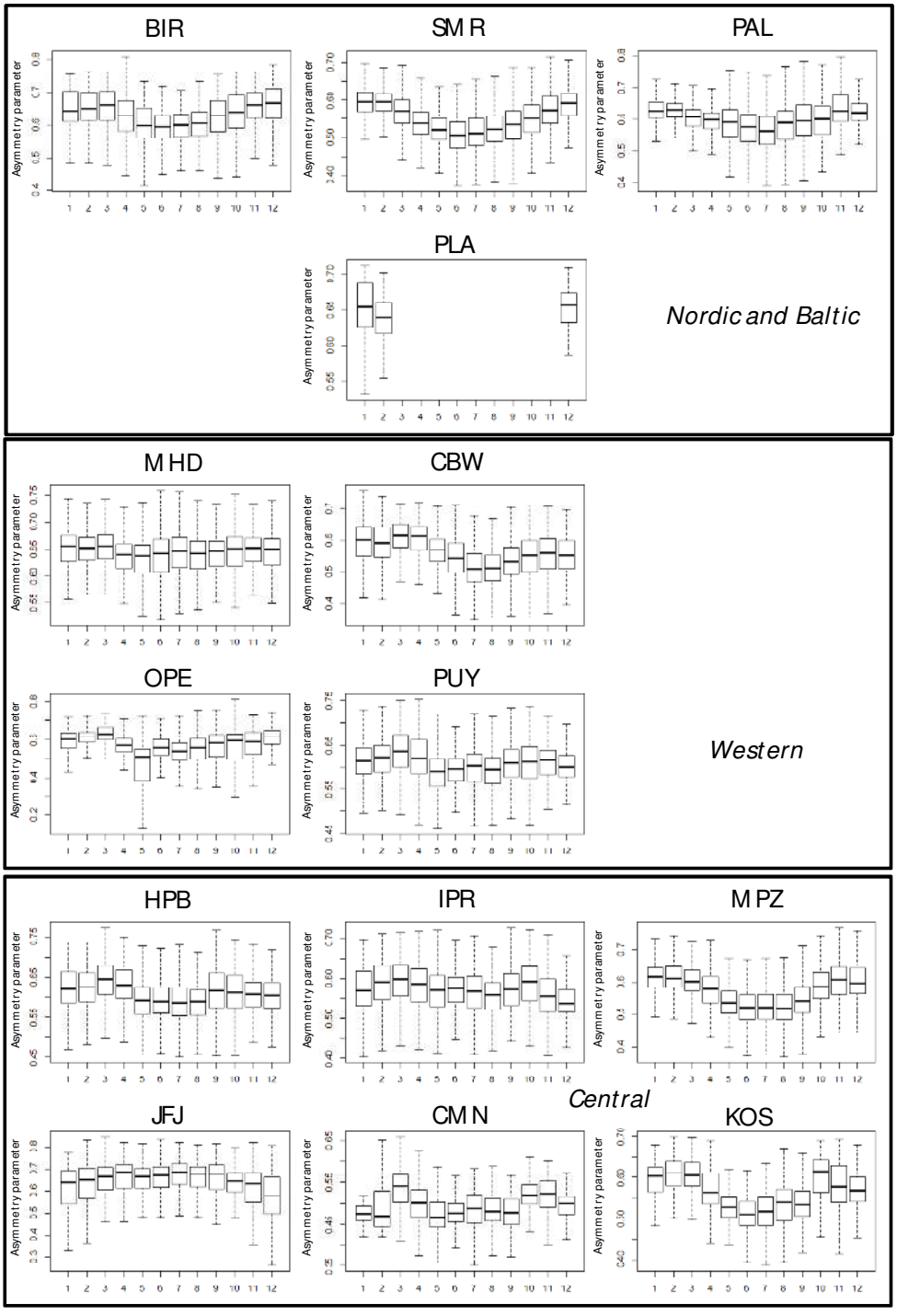

Figure 9: Seasonal cycles of *g* (calculated for the green wavelength).

Atmos. Chem. Phys. Discuss., https://doi.org/10.5194/acp-2017-826
Manuscript under review for journal Atmos. Chem. Phys.
Discussion started: 13 October 2017

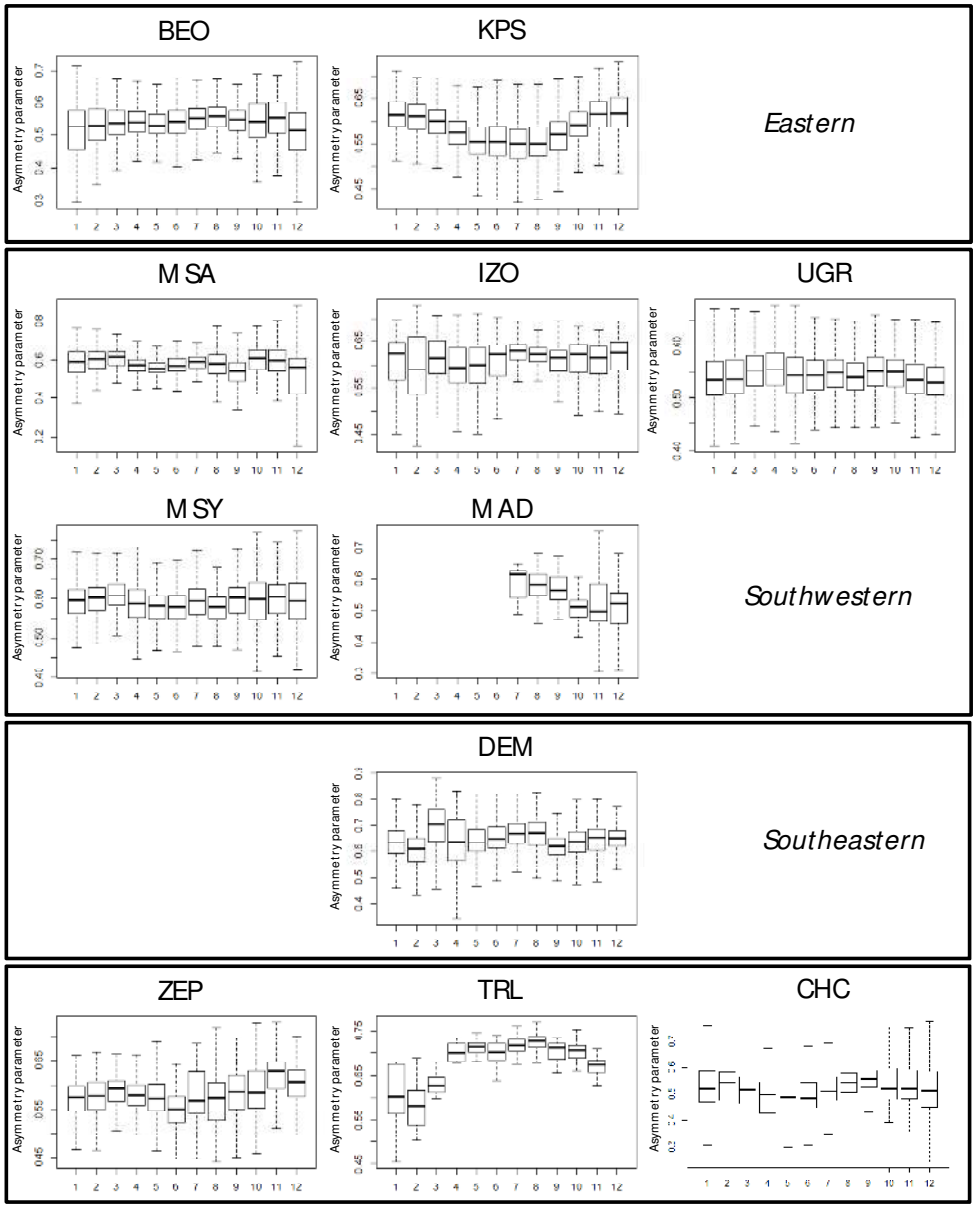

Figure 9: (Continued) Seasonal cycles of *g* (calculated for the green wavelength).